A multimodal RAGE-specific inhibitor reduces amyloid β–mediated brain disorder in a mouse model of Alzheimer disease

Rashid Deane,[1] Itender Singh,[1] Abhay P. Sagare,[1] Robert D. Bell,[1] Nathan T. Ross,[2,3] Barbra LaRue,[1] Rachal Love,[1] Sheldon Perry,[1] Nicole Paquette,[1] Richard J. Deane,[1] Meenakshisundaram Thiyagarajan,[1] Troy Zarcone,[4] Gunter Fritz,[5] Alan E. Friedman,[4] Benjamin L. Miller,[2,3] and Berislav V. Zlokovic[1,6]

[1]Center of Neurodegenerative and Vascular Brain Disorders, [2]Department of Biochemistry and Biophysics, [3]Department of Dermatology, and [4]Department of Environmental Medicine, University of Rochester, Rochester, New York, USA. [5]Department of Neuropathology, University of Freiburg, Freiburg, Germany. [6]Center for Neurodegeneration and Regeneration at the Zilkha Neurogenetic Institute and Department of Physiology and Biophysics, Keck School of Medicine, USC, Los Angeles, California, USA.

In Alzheimer disease (AD), amyloid β peptide (Aβ) accumulates in plaques in the brain. Receptor for advanced glycation end products (RAGE) mediates Aβ-induced perturbations in cerebral vessels, neurons, and microglia in AD. Here, we identified a high-affinity RAGE-specific inhibitor (FPS-ZM1) that blocked Aβ binding to the V domain of RAGE and inhibited Aβ40- and Aβ42-induced cellular stress in RAGE-expressing cells in vitro and in the mouse brain in vivo. FPS-ZM1 was nontoxic to mice and readily crossed the blood-brain barrier (BBB). In aged APP$^{sw/0}$ mice overexpressing human Aβ-precursor protein, a transgenic mouse model of AD with established Aβ pathology, FPS-ZM1 inhibited RAGE-mediated influx of circulating Aβ40 and Aβ42 into the brain. In brain, FPS-ZM1 bound exclusively to RAGE, which inhibited β-secretase activity and Aβ production and suppressed microglia activation and the neuroinflammatory response. Blockade of RAGE actions at the BBB and in the brain reduced Aβ40 and Aβ42 levels in brain markedly and normalized cognitive performance and cerebral blood flow responses in aged APP$^{sw/0}$ mice. Our data suggest that FPS-ZM1 is a potent multimodal RAGE blocker that effectively controls progression of Aβ-mediated brain disorder and that it may have the potential to be a disease-modifying agent for AD.

Introduction

Alzheimer disease (AD) is a neurodegenerative disorder associated with accumulation of amyloid β-peptide (Aβ) in brain (1). The amyloid hypothesis maintains that Aβ initiates a cascade of events leading to neuronal loss (2) and dementia (3). According to the vascular hypothesis of AD, initial vascular damage plays a critical role in neuronal damage (4–6) and Aβ accumulates in brain as a result of vascular injury (7). The vascular hypothesis proposes that blood-brain barrier (BBB) breakdown, causing accumulation in brain of multiple vasculotoxic and neurotoxic macromolecules and/or reductions in cerebral blood flow (CBF) and hypoxia, can initiate functional and structural changes in neurons before Aβ deposition occurs (7, 8). Importantly, BBB breakdown impairs vascular clearance of brain Aβ (7, 9) and may increase influx of peripheral Aβ into brain (10, 11), elevating brain Aβ levels. Reduced brain blood perfusion may also increase the expression and processing of Aβ-precursor protein (APP) (12–15), contributing to Aβ accumulation in brain. At pathophysiological levels, Aβ accelerates neurovascular (10, 16) and neuronal (17–19) dysfunction and self propagates (11, 20, 21), as in prion disease (22), leading to the development of cerebral β-amyloidosis (23).

The receptor for advanced glycation end products (RAGE) belongs to the immunoglobulin superfamily (24). RAGE contains an extracellular V domain that binds multiple ligands, including advanced glycation end products (AGE) proteins, S100/calgranulins, Aβ and amphoterin, 2 C-type immunoglobulin domains, and a short cytoplasmic domain that is required for RAGE-mediated signaling (25–27). The ligand-RAGE interactions lead to sustained cellular perturbation in chronic diseases, such as diabetes, inflammation, and AD (28–30). In AD, RAGE plays an important role as a cell-surface receptor for Aβ at the BBB, neurons, and microglia (7, 17, 25, 31). In brain endothelium, RAGE mediates influx of circulating Aβ into brain (10, 32) and of Aβ-laden monocytes across the BBB (33). In neurons, RAGE mediates Aβ-induced oxidant stress (17) and Aβ intraneuronal transport, causing mitochondrial dysfunction (19). Targeted expression of RAGE in neurons accelerates cognitive decline and Aβ-induced neuronal perturbation in APP transgenic mice (4). In microglia, RAGE amplifies Aβ-mediated inflammatory response (17). Importantly, RAGE expression in brain endothelium and neurons is substantially increased in an Aβ-rich environment (34), amplifying Aβ-induced pathogenic responses at the BBB and in brain.

Although preclinical data suggest that RAGE is an important therapeutic target in AD, anti-RAGE therapy has yet to be successfully developed for AD. Available anti-RAGE antibodies only block peripheral RAGE and do not cross the BBB (25, 30). Therefore, these agents cannot influence central Aβ processing. Similarly, soluble RAGE (sRAGE) does not cross the BBB either and at high pharmacological concentrations has been shown to reduce brain Aβ levels in young AD mice by sequestering plasma Aβ (10). However, its efficacy has not been confirmed in older AD mice with developed Aβ pathology, and its effect on cognitive performance
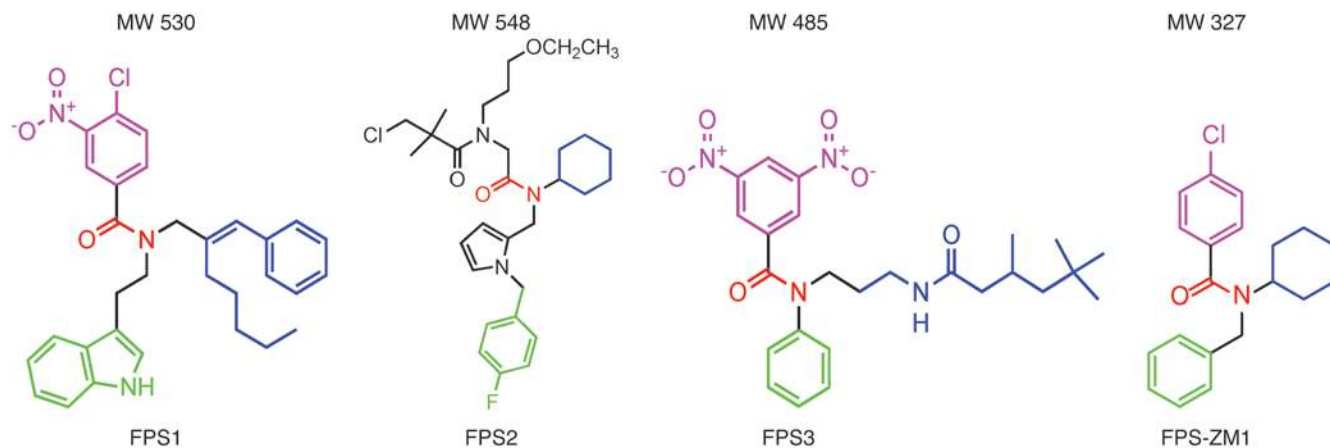
Figure 1
Structure of new high-affinity Aβ/RAGE blockers. FPS1, FPS2, and FPS3 derived from the primary screen. FPS-ZM1 derived from the secondary screen. Each structure shows the tertiary amide group (red) and its functional moieties, hydrophobic group (blue), electron-rich aromatic group (green), and electron-poor group (pink). For details see Results.

is unknown (10, 25, 30). No study to date reports whether small-molecule RAGE-specific inhibitors can mitigate Aβ-mediated brain disorder. Moreover, a phase 2 trial in AD patients with an azole-based first-generation small RAGE inhibitor has been terminated, likely because of toxicity observed at a higher therapeutic dose of the drug (35). Therefore, there is a need to develop new efficacious high-affinity Aβ/RAGE blockers that are safe and nontoxic.

To develop such an agent, we first screened a small molecule library and identified new tertiary amides that block Aβ/RAGE interaction with high affinity. We next synthesized a second-generation library of compounds based on the common structural features of the lead tertiary amides from the primary screen and identified a high-affinity RAGE-specific inhibitor, FPS-ZM1, which we show binds specifically to the V domain of RAGE, crosses the BBB, and inhibits Aβ-induced cellular stress in RAGE-expressing cells in vitro and in brain in vivo. Importantly, FPS-ZM1 was not toxic to cells and mice. In aged APP transgenic mice harboring the Swedish *APP* mutation (*APP$^{sw/0}$*) (36), FPS-ZM1 blocked RAGE actions at the BBB and in brain in vivo. At the BBB, FPS-ZM1 inhibited RAGE-mediated influx of circulating Aβ40 and Aβ42 into the brain. After crossing the BBB, FPS-ZM1 bound exclusively to RAGE in brain, which inhibited β-secretase activity and Aβ production and suppressed microglia activation and the neuroinflammatory response. Inhibition of RAGE actions at the BBB and in brain in vivo by FPS-ZM1 substantially reduced Aβ pathology and normalized CBF responses and cognitive performance in aged *APP$^{sw/0}$* mice.

Results

Primary screen for a high-affinity Aβ/RAGE inhibitor. Primary screen was performed using a diverse library of 5,000 small organic compounds (<600 Da) that were initially tested for their ability to inhibit Aβ/RAGE interaction in a receptor-binding assay using RAGE-transfected CHO cells (RAGE-CHO) and ^{125}I-Aβ40 as a ligand (33). As reported (33), RAGE was expressed between 24–48 hours of transfection (Supplemental Figure 1A; supplemental material available online with this article; doi:10.1172/JCI58642DS1). ^{125}I-Aβ40 binding to RAGE was concentration

dependent with a binding constant, K_d, of 75 ± 5 nM (Supplemental Figure 1B). Using a criterion that the inhibitory constant of a given inhibitor molecule, K_i, should not to be greater than 3 times K_d value for Aβ/RAGE binding, we identified 3 lead compounds named FPS1, FPS3, and FPS2. These lead compounds shared common structural characteristics, such as possessing a tertiary amide moiety substituted with a hydrophobic moiety and a monosubstituted electron-rich aromatic group (Figure 1). Linkage to the monosubstituted aromatic group was either direct (FPS3) or via an alkyl (FPS1) or heteroaromatic (FPS2) spacer. Two compounds featured a highly electron-poor substituted benzene ring (3-nitro, 4-chloro for FPS1, and 3, 5-dinitro for FPS3), while FPS2 had an N-alkylamidoacetyl group. Their K_i/K_d ratios were 2.78, 1.94, and 0.66, respectively (Table 1).

Secondary screen for a high-affinity Aβ/RAGE inhibitor. FPS2, the highest affinity Aβ/RAGE inhibitor from the primary screen, did not, however, cross the BBB in mice, and its uptake by brain was negligible (Table 1). Because of the restricted entry into the brain, we reasoned that systemically administered FPS2 will not inhibit RAGE in brain, but will inhibit RAGE at the luminal (blood-facing) side of the BBB because inhibition of luminal RAGE does not require penetration of a RAGE inhibitor into the brain. Since luminal RAGE at the BBB mediates influx of circulating Aβ into the brain (10), FPS2 was initially designated as an Aβ influx–selective RAGE blocker.

To generate a high-affinity RAGE blocker that can penetrate into the brain and block RAGE in additional CNS cell types, we synthesized a second-generation library of compounds based on the common structural features of the 3 lead compounds from the primary screen. The functional groups of the lead tertiary amides were altered to reduce the molecular weight to less than 450 Da and decrease the number of hydrogen bonds (Supplemental Figure 2), which are both predictive of higher BBB permeability (23, 37). The receptor-binding assay revealed 1 new second-generation compound out of 100 called FPS-ZM1 that had molecular weight of 327 Da and 1 H-bond (Figure 1). FPS-ZM1 inhibited Aβ/RAGE binding in CHO cells with approximately 2-fold greater affinity than its parent molecule, FPS2, as indicated by the respective K_i/K_d ratios of 0.66 and 0.34 (Table 1). Importantly, FPS-ZM1 had 53-

Table 1

Blocking properties, BBB permeability, percentage brain uptake, and toxicity of the lead Aβ/RAGE inhibitors from the primary screen (FPS1, FPS2, and FPS3), and the lead inhibitor from the secondary screen (FPS-ZM1)

RAGE inhibitor	K_i (nM)	K_i/K_d	PS product (μl/g/min)	Brain uptake (%)	Toxicity	
					In vitro (cells)	In vivo (mice)
FPS1	208 ± 12[A]	2.78 ± 0.17[A]	ND	ND	ND	ND
FPS3	146 ± 21[A]	1.94 ± 0.21[A]	ND	ND	ND	ND
FPS2	50 ± 9	0.66 ± 0.09	0.35 ± 0.10	0.71 ± 0.20	Not observed	Not observed
FPS-ZM1	25 ± 5[A]	0.34 ± 0.04[A]	18.67 ± 2.78	37.34 ± 5.56	Not observed	Not observed
Sucrose			0.17 ± 0.02	0.34 ± 0.04		

K_i, inhibitory constant of Aβ/RAGE binding in RAGE-transfected CHO cells; K_d, Aβ40-binding constant (75 ± 5 nM); B_{max}, maximal binding capacity (0.25 ± 0.03 nmoles/h/10^4 cells) in RAGE-transfected CHO cells. Data are taken from Supplemental Figure 1B BBB permeability is expressed as the PS product in mice. The PS product for sucrose is shown for comparison. Brain uptake is expressed as a percentage of the integrated plasma concentration. Toxicity of RAGE inhibitors was determined in CHO cells at 10 μM and in mice after 500 mg/kg i.p. injection. Values are mean ± SEM. n = 4–5 independent experiments per group. ND, not determined. [A]P < 0.05, for FPS1 and FPS3 compared with FPS2, and for FPS-ZM1 compared with FPS2. See Methods for details.

fold greater BBB permeability than FPS2 and its brain uptake was 37.3% compared with 0.71% for FSP2 determined within 20 minutes of an i.v. administration of both compounds (Table 1).

Chemically, FPS-ZM1 utilizes the same hydrophobic group as FPS2 (cyclohexyl; Figure 1 and Supplemental Figure 2) and is a tertiary amide, while incorporating many of the structural features of FPS1 and FPS3, such as an unsubstituted aromatic ring (analogous to FPS3, but attached to the tertiary amide via a methylene spacer rather than directly) and a para-chloro benzoyl group (analogous to that in FPS1, but lacking the meta-nitro group). This "hybrid" structure achieves a reduced molecular weight relative to FPS2 by deleting the heteroaromatic connector linking the electron-rich aromatic ring to the tertiary amide as well as by substituting the electron-poor aromatic ring for FPS2's complex N-(3-ethoxypropyl)-chloro t-butylamido group. Although all 3 groups may be required for inhibition of Aβ/RAGE binding, the structure-activity relationship studies with the second-generation compounds (Supplemental Figure 2) indicated that greater variation is tolerated in the hydrophobic moiety than in other groups. One can speculate that the polar chloride atom on the electron-poor aromatic group of FPS-ZM1 may enhance its binding to the receptor (38), contributing to its higher affinity as a Aβ/RAGE blocker compared with FPS2.

Cell-free assays with new RAGE inhibitors. Using a cell-free assay with immobilized sRAGE (25), we confirmed that FPS-ZM1 has approximately 2-fold greater potency to inhibit Aβ/RAGE binding than FPS2 (Figure 2A). In addition, FPS-ZM1 inhibited binding of other known RAGE ligands to sRAGE, including S100 calcium-binding protein B (S100B) and amphoterin (high mobility group box 1 [HMGB1]) (Figure 2B). However, the inhibitory constants for these ligands were significantly lower than for Aβ. Importantly, FPS-ZM1 bound only to immobilized sRAGE (Supplemental Figure 3A) and did not bind to immobilized Aβ (Supplemental Figure 3B) or other studied RAGE ligands (not shown). Since S100B, HMGB1, and Aβ bind to the V domain of RAGE (25, 31), these results have preliminarily suggested that FPS-ZM1 likely inhibits binding of ligands to the V domain of RAGE.

To determine whether FPS-ZM1 indeed binds to the V domain of RAGE, we have analyzed binding of ^{125}I-Aβ40 to the recombinant V domain and C1–C2 domains in the presence and absence of the inhibitory concentrations of FPS-ZM1. As reported, Aβ bound to the V domain, but not to the C1–C2 domains (31),

and its binding to the V domain was abolished by FPS-ZM1 (Figure 2C). Consistent with these data, FPS-ZM1 inhibited Aβ40 binding to sRAGE in the presence of C1 domain– and C2 domain–blocking antibodies, whereas a V domain–specific antibody blocked Aβ binding to sRAGE, as reported (31), preventing FPS-ZM1's inhibitory effect (Figure 2C). These data demonstrate that FPS-ZM1 specifically blocks Aβ binding to the V domain of RAGE.

Using a sensitive ELISA assay, we demonstrated that FPS-ZM1 does not inhibit Aβ40 and Aβ42 binding to another important Aβ receptor, i.e., the LDL receptor–related protein-1 (LRP) (Figure 2D), which is the major clearance receptor for Aβ at the BBB (9). Figure 2D shows no effect of FPS-ZM1 on Aβ binding to immobilized soluble LRP (sLRP), in contrast with almost complete inhibition of Aβ40 and Aβ42 binding by the receptor-associated protein (RAP), which blocks binding of Aβ and other LRP ligands to LRP/sLRP (9). The specificity of FPS-ZM1 binding to RAGE was subsequently confirmed in vivo (please see below).

Cell-based assays with new RAGE inhibitors. Before using FPS2 and FPS-ZM1 in cell-based assays, we determined whether these compounds are toxic to cells. Importantly, neither FPS2 nor FPS-ZM1 was toxic to cells at very high concentrations (Table 1 and Supplemental Figure 1C).

FPS-ZM1 was more potent than FPS2 in inhibiting Aβ-induced generation of thiobarbituric acid–reactive substances (TBARS) in RAGE-CHO cells, reflecting its greater ability to inhibit lipid peroxidation in cell membranes (ref. 17 and Figure 2E), as indicated by the respective EC_{50} values of 28 ± 6 and 11 ± 2 nM. Consistent with these findings, FPS-ZM1 was more effective than FPS2 in reducing an overall Aβ/RAGE-mediated cellular oxidative stress (Supplemental Figure 4A). Similarly, FPS-ZM1 was more effective as an NF-κB inhibitor, as indicated by a greater reduction of Aβ-induced NF-κB nuclear translocation in RAGE-CHO cells compared with FPS2 (Figure 2F and Supplemental Figure 4B).

It has been shown that NF-κB inhibitors block Aβ production (39) and that NF-κB inhibition transcriptionally downregulates the β-site APP-cleaving enzyme 1 (BACE1 or β-secretase) in astrocytes and neural cells in the presence of Aβ (40). In addition, AGEs/RAGE interaction has been shown to upregulate BACE1 in neural cells via NF-κB activation (41). Therefore, we asked whether our RAGE blockers can inhibit BACE1 in RAGE-expressing SH-SY5Y neural cells in the presence of oligomeric Aβ. Our
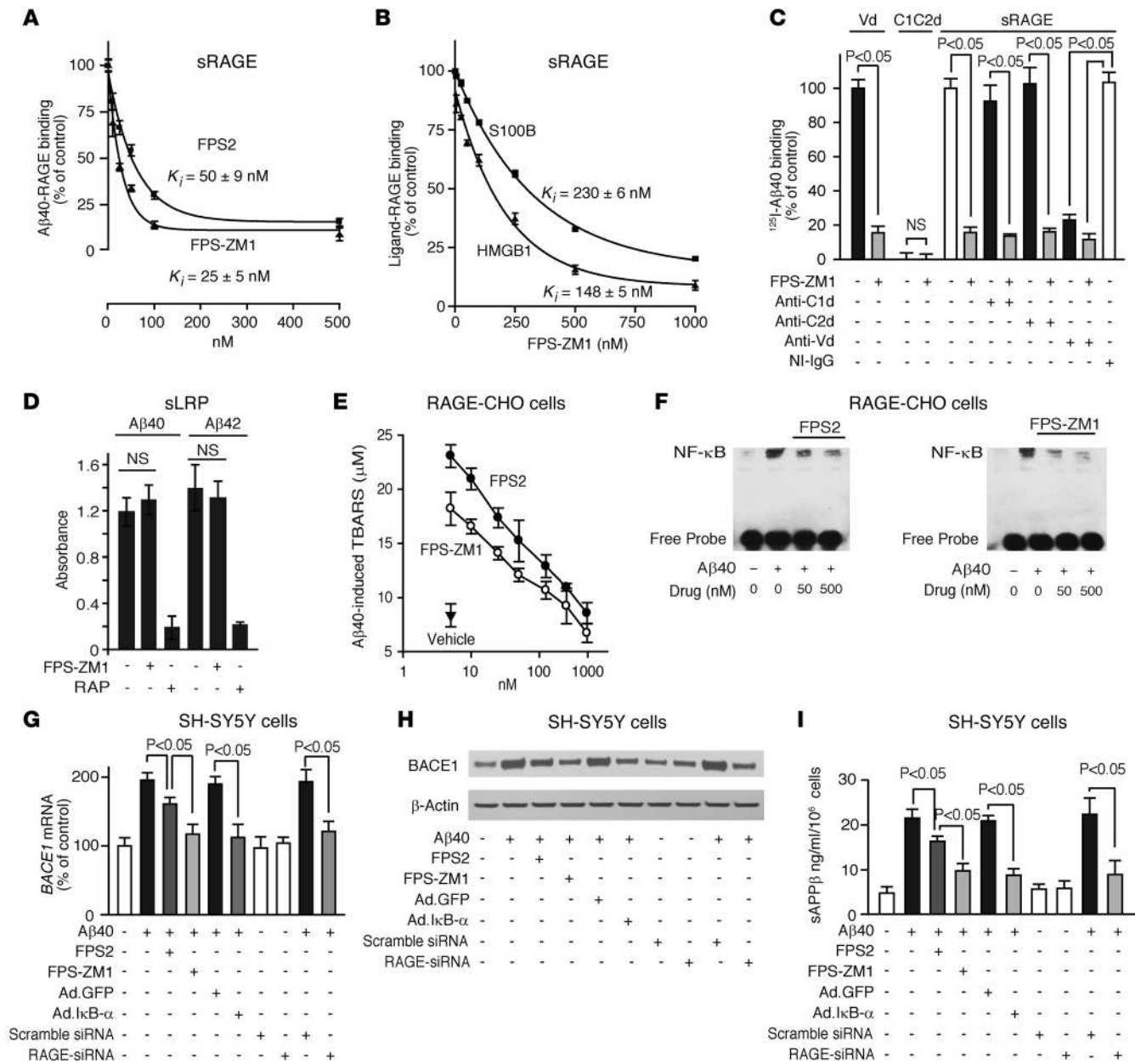
Figure 2

FPS-ZM1 and FPS2 inhibit Aβ/RAGE binding in cell-free and cell-based assays. (**A**) ^{125}I-Aβ40 (5 nM) binding to immobilized human sRAGE in the presence of FPS2 or FPS-ZM1 (10–500 nM). (**B**) ^{125}I-HMGB1 (5 nM) or ^{125}I-S100B (5 nM) binding to sRAGE in the presence of FPS-ZM1 (10–1,000 nM). In **A** and **B**, K_i represents inhibitory constant. (**C**) ^{125}I-Aβ40 (5 nM) binding to immobilized human recombinant RAGE V domain (Vd) or C1C2 domain (C1C2d) with and without FPS-ZM1 (200 nM) and to sRAGE with and without RAGE-specific C1 domain (anti-C1d), C2 domain (anti-C2d), or V domain (anti-Vd) antibodies (20 μg/ml), NI-IgG, and FPS-ZM1 (100 nM). (**D**) Aβ40 and Aβ42 binding to immobilized human sLRP with and without FPS-ZM1 (1 μM) or RAP (1 μM). (**E**) Aβ40-induced (1 μM) TBARS in RAGE-CHO cells in the presence of vehicle (closed triangle) or various concentrations of FPS2 (white circles) and FPS-ZM1 (black circles). (**F**) Aβ40-induced (1 μM) NF-κB activation in RAGE-CHO cells with and without FPS2 and FPS-ZM1. (**G**–**I**) *BACE1* mRNA (**G**), BACE1 protein (**H**), and secreted sAPPβ (**I**) levels determined by qRT-PCR, immunoblotting, and ELISA, respectively, in SH-SY5Y cultures treated with vehicle or Aβ40 (1 μM) with or without FPS2 or FPS-ZM1 (50 nM) after transduction with Ad. GFP or a mutant Ad. IκB-α (S32, 36A), and/or transfection with scrambled siRNA or RAGE-siRNA. All values are means ± SEM. *n* = 3–5 independent experiments. β-actin was used as a loading control in **H**.

data show that FPS-ZM1 was more effective than FPS2 in reducing Aβ40-induced increases in *BACE1* mRNA and protein levels (Figure 2, G and H, and Supplemental Figure 4C) and the generation of sAPPβ, an APP cleavage product of BACE1 (Figure 2I)

indicative of BACE1 activity (42). We next showed that FPS2 and FPS-ZM1 reduced nuclear p65 NF-κB levels in neural cells by 30% and 95%, respectively, and that the efficacy of a relatively low concentration of FPS-ZM1 was comparable to inhibition of NF-κB

obtained with a mutant form of IκB-α (S32, 36A) (Supplemental Figure 4D), a potent suppressor of NF-κB gene expression (40). Moreover, RAGE inhibition by siRNA (Supplemental Figure 4E) abolished the effect of Aβ40 on BACE1 (Figure 2, G–I), confirming that RAGE is critical for Aβ-induced BACE1 activation.

To complement data in Figure 2 that show mainly how RAGE inhibitors block Aβ40 effects on RAGE in cell-based assays, we have performed similar experiments with Aβ42. These experiments indicated that FPS-ZM1 blocks Aβ42 binding to RAGE and Aβ42-induced TBARS formation in RAGE-CHO cells as well as Aβ42-induced increase in *BACE1* mRNA and secreted sAPPβ levels in SH-SY5Y cells (Supplemental Figure 5), confirming that FPS-ZM1 blocks interaction of both Aβ40 and Aβ42 with cell-surface RAGE.

Toxicity studies in mice. Before evaluating the effects of RAGE blockers in *APP*[sw/0] mice, we determined whether they are toxic to mice. Toxicity data indicated no changes in physiological functions (heart rate, BP, respiration rate), blood gasses and pH, glucose levels, and hepatic and renal functional tests at a dose of FPS2 and FPS-ZM1 that was 500-fold higher than the therapeutic dose of 1 mg/kg i.p. utilized in *APP*[sw/0] mice (Table 1). For example, all functional liver tests (Idexx Reference Laboratories mouse code 60405), including plasma levels of aspartate aminotransferase, alanine aminotransferase, alkaline phosphatase, albumin, and total proteins, were within physiological range in *APP*[sw/0] mice dosed with FPS-ZM1.

In addition, we have not observed an increased rate of infection in 15- to 17-month-old *APP*[sw/0] mice treated with FPS-ZM1. Mice treated with high doses of FPS-ZM1 (i.e., 500 mg/kg) had normal differential white blood cell counts (neutrophils, monocytes, eosinophiles, basophiles, lymphocytes) and showed no histological changes in organs normally expressing RAGE (e.g., lung, liver, kidney).

FPS2 and FPS-ZM1 inhibit in vivo RAGE-mediated Aβ BBB transport in APP[sw/0] *mice.* In order to determine whether our designated influx-sensitive FPS2 blocker and the multimodal FPS-ZM1 can inhibit RAGE-mediated Aβ transport across the BBB in *APP*[sw/0] mice in vivo, we used an arterial vascular brain perfusion technique to quantify influx of circulating Aβ into the brain, as reported (10, 43). First, we reproduced earlier findings (10, 43) demonstrating that Aβ40 transport across the BBB of AD mice is RAGE mediated. We showed that a RAGE-specific antibody that does not cross the BBB blocks Aβ40 transport across the BBB by inhibiting RAGE at the luminal side of brain endothelium in contrast with nonimmune (NI) IgG (Figure 3A). sRAGE sequestered circulating Aβ and abolished its transport into the brain (data not shown), as reported (10). Next, we showed that both FPS2 and FPS-ZM1 inhibit RAGE-mediated Aβ40 influx across the BBB in 15- to 17-month-old *APP*[sw/0] mice by 93% and 97%, respectively (Figure 3A), providing evidence that these drugs block RAGE at the luminal side of the BBB in brain in vivo. We then designed an acute experiment in which FPS-ZM1 was preincubated with either sRAGE or sLRP prior to infusion into the brain circulation of 15- to 17-month-old *APP*[sw/0] mice. This study indicated that preincubation of FPS-ZM1 with sRAGE, but not with sLRP, abolishes the effect of the drug on Aβ transport (Figure 3A), indicating that binding of FPS-ZM1 to sRAGE before infusion cancels out the effect of the drug on Aβ40 influx into the brain in vivo. These data are consistent with in vitro data showing binding of FPS-ZM1 to sRAGE (Figure 2, A and C), but not to immobilized sLRP (Figure 2D).

To test whether FPS-ZM1 can inhibit influx into the brain across the BBB of Aβ42, we performed an experiment as in Figure 3A infusing Aβ42 into the brain circulation of *APP*[sw/0] mice using brain perfusion technique (43). These data showed that FSP-ZM1 blocks influx of Aβ42 into the brain to a level roughly equivalent to FPS-ZM1 inhibition of Aβ40 influx (Supplemental Figure 6), consistent with the observations that RAGE mediates influx of both Aβ40 and Aβ42 into the brain (10).

FPS-ZM1 binds in vivo to RAGE in brains of APP[sw/0] *mice.* Because FPS-ZM1 accumulates in the brain after crossing the BBB (Table 1), we next determined whether this drug binds to RAGE in brain in vivo and can therefore act to block RAGE actions in brain, as shown in multiple cell-free and cell-based assays and at the BBB in vivo. Our data show that after crossing the BBB, FPS-ZM1 binds exclusively to RAGE in brain, as demonstrated by co-IP of FPS-ZM1 with RAGE from brains of 15-month-old *APP*[sw/0] mice, namely, FPS-ZM1 was found only in RAGE-IP fraction from brain after systemic administration (Figure 3B). We also show that after systemic administration, FPS-ZM1 was undetectable in RAGE-depleted brain fraction (Figure 3C) that contains other Aβ receptors, such as the essential Aβ vascular clearance receptor LRP (9). These data additionally confirm that FPS-ZM1 binds exclusively to RAGE in brain in vivo.

As reported in Table 1, under the same experimental conditions, FPS2 was undetectable in brain and did not penetrate across the BBB.

Together, these data indicate that FPS-ZM1 can inhibit RAGE both at the BBB and in brain in vivo, whereas the influx-selective RAGE blocker FPS1 inhibits RAGE only at the BBB, which eliminates influx of circulating Aβ into the brain.

Therapy of aged APP[sw/0] *mice with new RAGE inhibitors.* Next, we tested the effects of both RAGE inhibitors in 15- to 17-month-old *APP*[sw/0] mice. These mice develop Aβ and amyloid load in brain approximately 1 order of magnitude greater than that of young AD mice used in an earlier study with sRAGE, which acts to bind peripheral Aβ in plasma (10).

In the present study, 15- to 17-month-old *APP*[sw/0] mice were randomized into 2 experimental groups receiving either the influx-selective FPS2, which does not cross the BBB (Table 1) but can inhibit RAGE-mediated influx of Aβ into the brain (Figure 3A), or multimodal FPS-ZM1, which, in addition to inhibiting RAGE at the BBB (Figure 3A and Supplemental Figure 6), also crosses the BBB and binds to RAGE in brain (Table 1 and Figure 3, B and C). Mice received 1 mg/kg i.p. daily of either compound for 2 months beginning at 15 months of age (Figure 3). Control group received vehicle. In all studied assays, FPS-ZM1 showed superior beneficial effects compared with FPS2, indicating that penetration of a RAGE blocker into the brain and blockade of RAGE actions in the brain critically augments the benefit of anti-RAGE therapy compared with blockade of RAGE-mediated Aβ influx only. For example, FPS2 and FPS-ZM1 reduced Aβ40 and Aβ42 levels in the cortex and hippocampus by 30%–40% and 60%–80%, respectively (Figure 3, D and E). Consistent with these findings, FPS-ZM1 had superior effects on reducing Aβ load (not shown) and amyloid load in the cortex and hippocampus by 70%–80% (Figure 3F). Neither FPS2 nor FPS-ZM1 caused cerebral microhemorrhages (data not shown), in contrast with some forms of anti-Aβ therapy (44). Remarkably, FPS-ZM1 almost completely restored the CBF response with whisker stimulation in older *APP*[sw/0] mice (Figure 3G) in contrast with FPS2, which was marginally effective. FPS-ZM1 completely restored the behavioral responses determined by
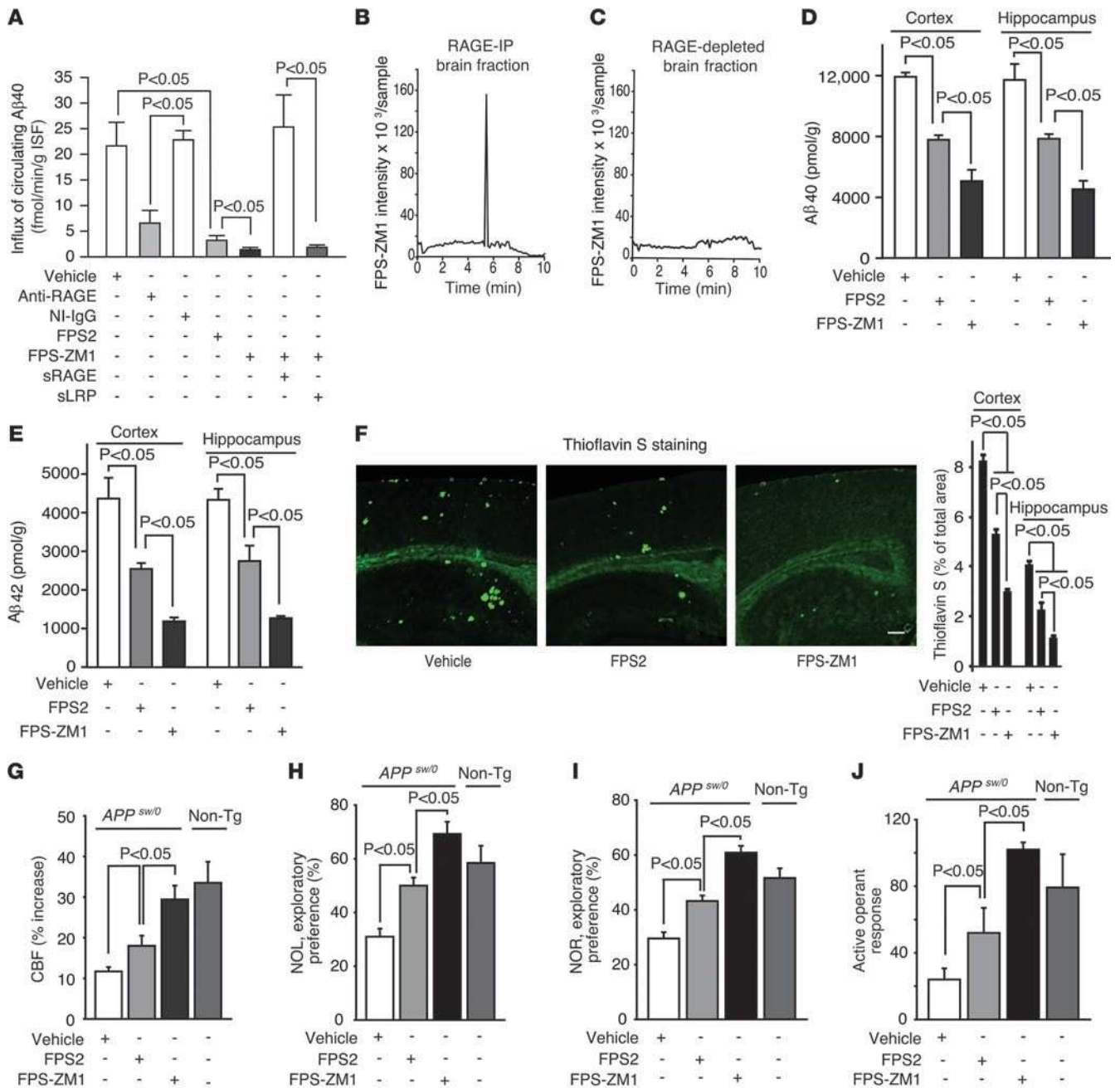
Figure 3

FPS-ZM1 and FPS2 block RAGE-mediated Aβ BBB transport, Aβ pathology, and functional outcome in old $APP^{sw/0}$ mice. (**A**) Influx of circulating ^{125}I-Aβ40 (1.5 nM) across the BBB in 15- to 17-month-old $APP^{sw/0}$ mice with and without anti-RAGE antibody (40 μg/ml), NI IgG (40 μg/ml), FPS2 (200 nM), or FPS-ZM1 (200 nM) alone or after preincubation with sRAGE or sLRP. Values are mean ± SEM; $n = 4–6$ mice per group. (**B** and **C**) Detection of FPS-ZM1 in the brain of 15 month old $APP^{sw/0}$ mice 5 minutes after an I.V. administration. FPS-ZM1 was found in RAGE-IP brain fraction (**B**), but not in RAGE-depleted brain (**C**). Representative results from 6 experiments are shown. (**D** and **E**) Aβ40 (**D**) and Aβ42 (**E**) levels in the cortex and hippocampus. (**F**) Thioflavin S–positive amyloid deposits in the brain (left) and quantification of thioflavin S–positive area in the cortex and hippocampus (right). Scale bar: 350 μm. (**G–J**) CBF response to whisker stimulation (**G**), NOL (**H**), NOR (**I**), and active operant response (**J**) in 15-month-old $APP^{sw/0}$ mice treated with vehicle, FPS2, or FPS-ZM1 for 2 months. Nontransgenic littermate controls (gray columns) are shown in panels **G–J**. Values are mean ± SEM. $n = 4–6$ mice per group.

novel object location (NOL) and novel object recognition (NOR) tests (Figure 3, H and I) and active operant learning (Figure 3J) in older $APP^{sw/0}$ mice. In contrast, nonpenetrating FPS2 had only moderate effects on behavior.

Based on data showing that RAGE inhibitors block Aβ/RAGE-mediated increase in BACE1 in neural cells in vitro (Figure 2, G–I) and that neurons in $APP^{sw/0}$ mice express RAGE (19), as confirmed in this study (data not shown), we hypothesized that blockade of
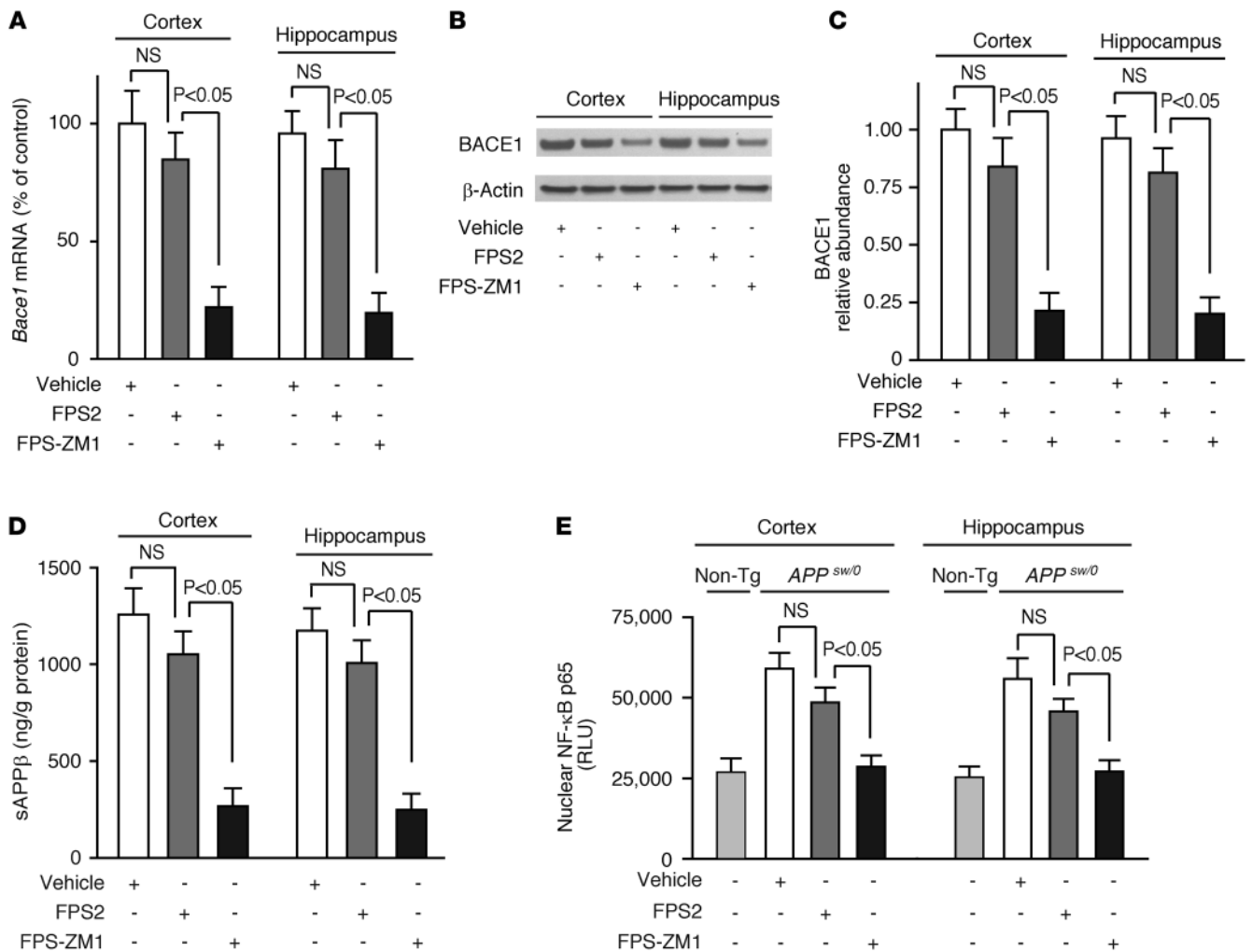
Figure 4
Effects of FPS-ZM1 and FPS2 on BACE1 in brains of 17-month-old *APP^sw/0* mice. (**A–D**) *Bace1* mRNA (**A**), BACE1 protein (**B** and **C**), and sAPPβ (**D**) levels determined in the cortex and hippocampus by qRT-PCR, immunoblotting, and ELISA, respectively. Quantitative densitometry was used to determine relative abundance of BACE1 using β-actin as a loading control. (**E**) Nuclear NF-κB p65 relative levels in the cortex and hippocampus. *APP^sw/0* mice were treated with vehicle, FPS2, or FPS-ZM1 for 2 months starting at 15 months of age. Non-Tg, nontransgenic littermate controls. Values are mean ± SEM. *n* = 5–6 mice per group.

RAGE in neurons by FPS-ZM1 in vivo will inhibit BACE1 and Aβ production in 17-month-old *APP^sw/0* mice, whereas nonpenetrating FPS2 will not have an effect on BACE1 in brain. Indeed, FPS-ZM1 reduced *BACE1* mRNA and protein levels and sAPPβ levels in the cortex and hippocampus of 17-month-old *APP^sw/0* mice by more than 80% compared with modest, but nonsignificant, effects of FPS2 (Figure 4, B–D). As reported (45), there was a significant, approximately 2-fold, increase in nuclear p65 NF-κB levels in the cortex and hippocampus of 17-month-old *APP^sw/0* mice compared with age-matched nontransgenic controls (Figure 4E). Consistent with earlier reports showing that NF-κB inhibition blocks Aβ production and transcriptionally downregulates BACE1 in astrocytes and neural cells in the presence of Aβ (39, 40) and that ligand/RAGE interaction upregulates BACE1 in neural cells via NF-κB activation (41), we found that the effect of FPS-ZM1 on BACE1 in brain of *APP^sw/0* mice was associated with complete normalization of nuclear p65 NF-κB levels compared with nontransgenic

littermate controls (Figure 4E). On the other hand, nonpenetrating FPS2 had a modest, insignificant effect on p65 NF-κB levels (Figure 4E). Consistent with these results, FPS-ZM1 substantially reduced oxidative stress in neurons and other brain cells in 17-month-old *APP^sw/0* mice, whereas FPS2 had a relatively modest effect (Supplemental Figure 7).

Finally, we studied whether RAGE inhibitors can influence the neuroinflammatory response. Our data show that FPS-ZM1 reduced the number of activated microglia in brains of 17-month-old *APP^sw/0* mice by approximately 80% compared with a moderate 25% reduction by FPS2 (Figure 5, A and B), which was proportional to their respective reductions of Aβ and amyloid levels in brain (Figure 3, D–G). As reported (46), RAGE was abundantly expressed in microglia in *APP^sw/0* mice (not shown). Consistent with these findings, FPS-ZM1 substantially suppressed the mRNA and protein levels of different proinflammatory cytokines, including TNF-α, IL-1β, IL-6, and MCP-1 in the cortex and hippocampus
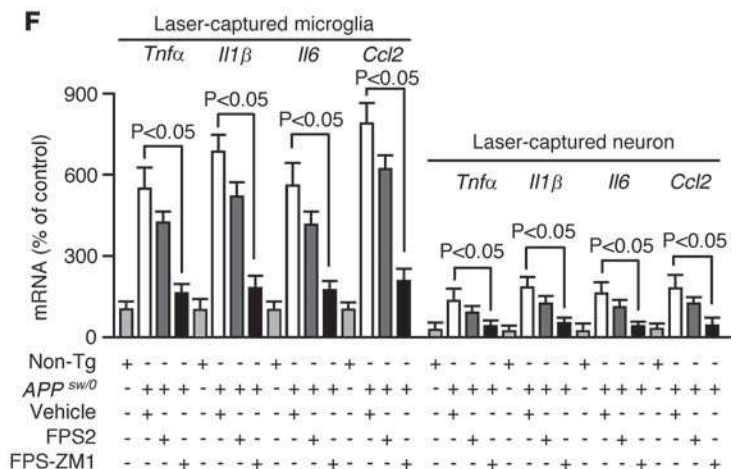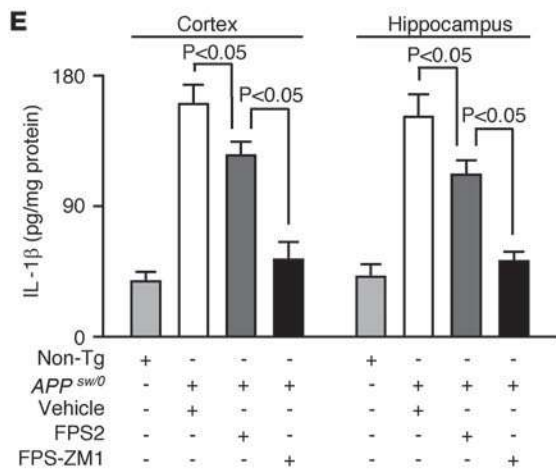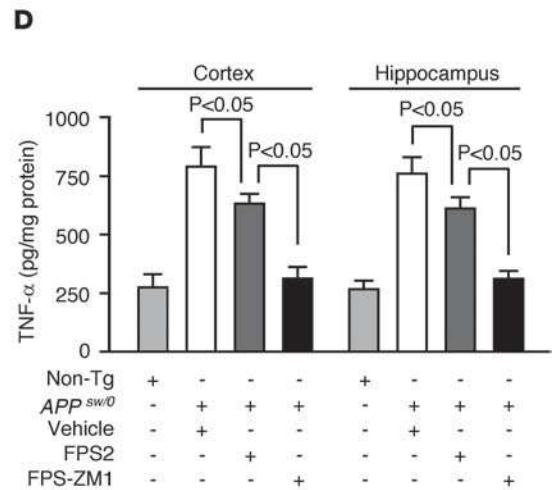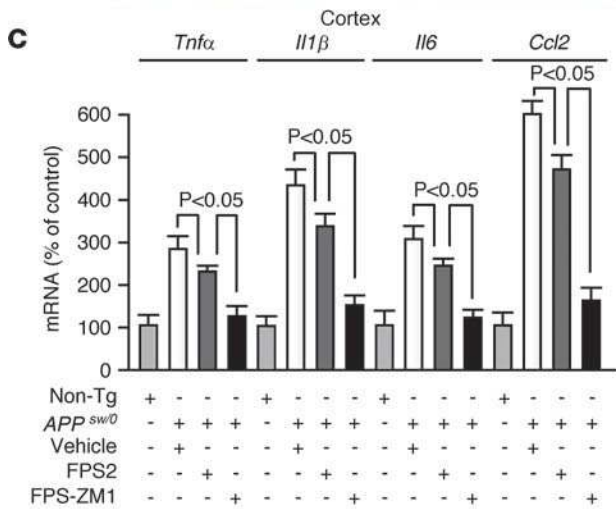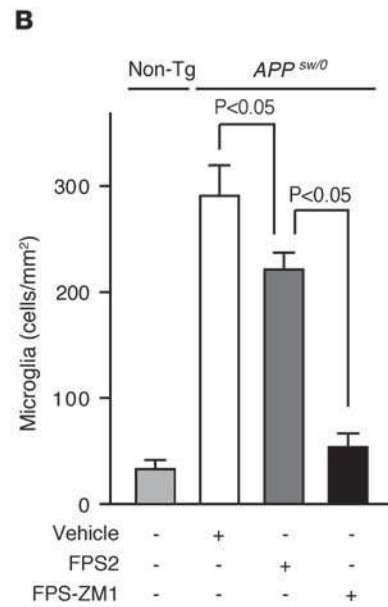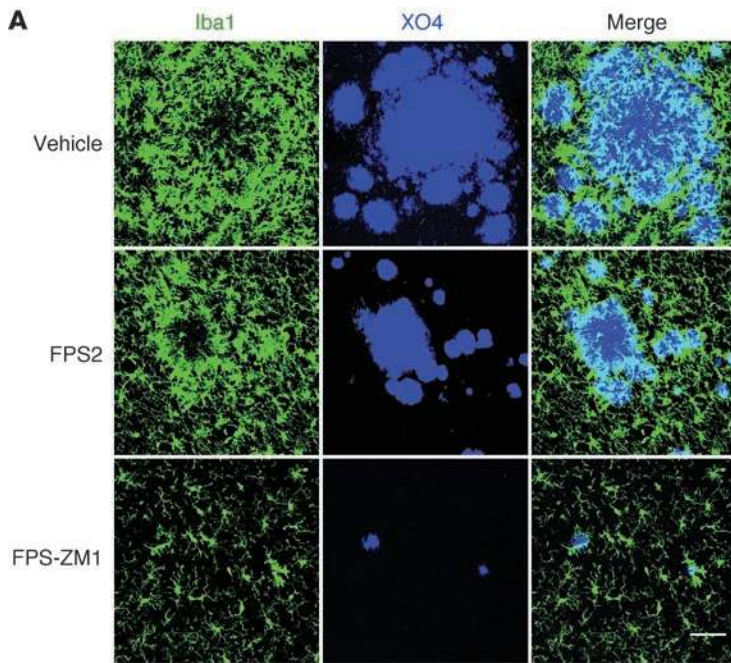
Figure 5
FPS-ZM1 and FPS2 control the neuroinflammatory response in 17-month-old $APP^{sw/0}$ mice. (**A**) Confocal microscopy analysis of Iba1-positive microglia (green) and methoxy X04–positive amyloid-β (blue) and merged images. Scale bar: 50 μm. (**B**) Microglia numbers in the cortex. (**C–E**) Relative mRNA expression levels of $Tnf\alpha$, $Il1\beta$, $Il6$, and $Ccl2$ determined by qRT-PCR (**C**), TNF-α (**D**), and IL-1β (**E**) protein levels determined by ELISA in the cortex and hippocampus. (**F**) Relative mRNA expression levels of $Tnf\alpha$, $Il1\beta$, $Il6$, and $Ccl2$ in laser-captured microglia and neurons determined by qRT-PCR. $APP^{sw/0}$ mice were treated with vehicle, FPS2, or FPS-ZM1 for 2 months starting at 15 months of age. Values are mean ± SEM. n = 5 mice per group.

of $APP^{sw/0}$ mice by 70%–80% compared with 20%–25% reductions with FPS2 (Figure 5, C–E). Comparable reductions in the mRNA levels of these these cytokines were found in laser-captured microglia from the cortex and hippocampus of 17-month-old $APP^{sw/0}$ mice (Figure 5F). The relative levels of mRNA transcripts for cytokines in laser-captured microglia were by 5- to 6-fold higher than in laser-captured neurons from the same $APP^{sw/0}$ mice. Consistent with these data, FPS-ZM1 vigorously inhibited Aβ/RAGE-mediated NF-κB–dependent increase in the mRNA and protein levels of different proinflammatory cytokines in the RAGE-expressing murine microglia BV-2 cell line (Supplemental Figure 8).

Discussion

Screening a second-generation library of small compounds that were synthesized based on the common structural features of the lead tertiary amides from an initial primary screen, we have identified a high-affinity RAGE-specific blocker, FPS-ZM1, which we show binds specifically to the V domain of RAGE and inhibits Aβ40- and Aβ42-induced cellular stress in RAGE-expressing cells in vitro and in brain in vivo. FPS-ZM1 effectively controlled progression of an Aβ-mediated brain disorder and the related neurovascular and cognitive dysfunction in 17-month-old $APP^{sw/0}$ mice with fully developed Aβ and amyloid pathology by blocking RAGE actions at the BBB and in brain. This has resulted in inhibition of circulating Aβ influx into the brain, on the one hand, and inhibition of BACE1 and Aβ production in brain and suppression of the neuroinflammatory response on the other. The present anti-RAGE therapy with FPS-ZM1 did not influence, however, protective Aβ vascular clearance because FPS-ZM1 did not bind to LRP, a key receptor at the BBB-mediating efflux of Aβ from brain to blood (9).

As with other multimodal neurovascular medicines (7), FPS-ZM1 likely blocked multiple RAGE-mediated pathways in $APP^{sw/0}$ mice simultaneously. A comparison between FPS2, an "influx-selective" Aβ RAGE blocker, which we show specifically inhibits RAGE at the BBB and RAGE-mediated Aβ influx across the BBB, but does not inhibit RAGE in brain because it does not cross the BBB, and a multimodal FPS-ZM1 that blocks RAGE actions at the BBB and in brain indicates that blocking Aβ influx alone may account for approximately 50% of the benefit observed with the multimodal anti-RAGE therapy with FPS-ZM1. For example, both FPS2 and FPS-ZM1 effectively blocked RAGE at the BBB, resulting in approximately 95% inhibition of Aβ influx into the brain. However, only FPS-ZM1, which crosses the BBB, efficiently blocked RAGE-dependent BACE1 expression and activity in brain of 17-month-old $APP^{sw/0}$ mice in contrast with a marginal, insignificant effect of FSP2. These differential effects of the 2 RAGE blockers resulted in a striking difference in their respective thera-

peutic effects on Aβ40 and Aβ42 levels in the cortex and hippocampus of 17-month-old $APP^{sw/0}$ mice, i.e., 30%–40% reductions with FPS2 compared with 60%–80% reductions with FPS-ZM1. Consistent with these findings, the nonpenetrating FPS2 had moderate effects on CBF responses to whisker stimulation, behavior, and neuroinflammation, whereas the multimodal FPS-ZM1 completely restored the blood flow and behavioral responses and blocked the neuroinflammatory response by approximately 85%.

In contrast with leaky vessels in peripheral organs (47), the BBB restricts entry of polar molecules into the brain. However, nutrients such as glucose, amino acids, and vitamins cross the BBB using specific transporters (48). Peptides in general poorly cross the BBB (49, 50), but can be transported into the brain if specific transporters and/or receptors with a transport function are expressed in brain endothelium either under physiological (51, 52) or pathological conditions, as in the case of RAGE and Aβ transport (43). Recent studies have independently confirmed earlier observations that circulating Aβ is an important precursor for brain Aβ (7, 10, 33) by demonstrating that peripheral Aβ can accelerate cerebral β-amyloidosis in a mouse model (11) and that liver serves as an important source of brain Aβ (53). These recent findings have extended earlier work showing that circulating Aβ enters the brain via RAGE-mediated transport across the BBB, either as a soluble molecule (10) and/or via Aβ-laden monocytes (33), and contributes to the formation of parenchymal amyloid plaques, as shown, for example, in nonhuman primates (54). Thus, blocking RAGE at the BBB by FPS2 and FPS-ZM1 eliminates contributions of peripheral Aβ to brain Aβ, as shown in $APP^{sw/0}$ mice. Because sRAGE is not present in plasma, as shown in nondiabetic and diabetic mice (55) or $APP^{sw/0}$ mice in this study, blockade of peripheral Aβ influx into the brain by FPS-ZM1 or FPS2 is independent of sRAGE.

In vitro studies in cultured neural cells have shown that FPS-ZM1 effectively inhibits Aβ-induced, RAGE-dependent NF-κB–mediated transcriptional activation of BACE1, a key enzyme involved in generation of Aβ (42). We also found that reduced Aβ40 and Aβ42 levels and BACE1 expression and activity in brains of FPS-ZM1–treated $APP^{sw/0}$ mice were coincidental with blockade of NF-κB and normalization of NF-κB activity, which is otherwise increased by approximately 2-fold compared with that in nontransgenic controls (45), also confirmed in this study. These findings are in agreement with previous reports demonstrating NF-κB–dependent Aβ production (39, 40) and RAGE-mediated BACE1 upregulation (41).

It is conceivable that FPS-ZM1 can protect neurons from Aβ-induced, RAGE-dependent oxidative stress and mitochondrial injury (17, 19, 56) by directly blocking Aβ/RAGE interaction in neurons and/or by blocking it indirectly by reducing Aβ levels in brain. FPS-ZM1 also blocks binding of other ligands to RAGE, such as S100B, AGE, and HMGB1, which have been suggested to contribute to RAGE-mediated long-term tissue damage in models of diabetes, immune/inflammatory disorders, and AD (25). Although the relative contribution of S100, AGE, or HMGB1 to neuronal injury and neurovascular dysfunction in $APP^{sw/0}$ mice is likely minor compared with Aβ, blocking possible pathogenic effects of these RAGE ligands in AD will likely have an added benefit to anti-RAGE therapy with FPS-ZM1.

Besides direct neuronal protective effects, FPS-ZM1 may indirectly protect neurons by suppressing Aβ/RAGE-induced microglia activation and NF-κB–dependent expression of microglia-derived proinflammatory cytokines, which have been shown to contribute

to secondary neuronal injury (10, 17). A remarkable antiinflammatory activity of FPS-ZM1 in *APPsw/0* mice was likely related to direct inhibition of RAGE in microglia, as supported by data in cultured microglia, but was also proportional to elimination of Aβ and amyloid load. The exact role of microglia in AD and AD models, however, is complex and could be beneficial through the clearance function of amyloid (57, 58) and/or harmful, given that microglia are the major source of proinflammatory cytokines that can contribute to neuronal injury (59).

In summary, we have demonstrated that FPS-ZM1, a new next-generation RAGE inhibitor, in addition to being an Aβ-lowering agent, can also block multiple mechanisms of Aβ-induced cellular stress in RAGE-expressing brain endothelium, neurons, and microglia in vitro and in brain in vivo, which can directly control neurovascular and cognitive dysfunction. Importantly, FPS-ZM1 is effective at an age in which Aβ accumulation and functional deficits have firmly been established in *APPsw/0* mice. Increased expression of RAGE in blood vessels, neurons, and microglia in brains of AD-affected individuals indicates that RAGE is relevant to the pathogenesis of neurovascular and neuronal dysfunction and death in this disease. Therefore, this RAGE inhibitor holds translational potential to control disease progression in individuals diagnosed with AD who have already developed cerebral Aβ accumulations and the associated neurovascular and cognitive deficits. We suggest it could be developed in the future as a disease-modifying agent for patients diagnosed with AD.

Methods

Screening for Aβ/RAGE inhibitors

RAGE-CHO cells. CHO cells were maintained in Ham's F12 medium, supplemented with 10% FBS, 2 mM glutamine, 100 U/ml penicillin G, and 0.1 mg/ml streptomycin (Invitrogen) at 37°C and 5% CO_2. Human RAGE cDNA (a gift from Shi Du Yan, Columbia University, New York, New York, USA) was cloned into pcDNA vector (Invitrogen) and purified using EndoFree Plasmid Maxi Kit (QIAGEN). Transfections of CHO cells with pcDNA3-RAGE were performed in 70%–80% confluent monolayers with lipofectamine (Invitrogen) following the manufacturer's instructions. RAGE-CHO cells were used in Aβ-binding studies and other in vitro assays within 24 hours of transfection. pcDNA3-GFP was used as a mock transfection control.

Library of compounds. A diverse library of 5,000 small organic compounds (Albany Molecular Research) was used for the primary screen. All compounds were prefiltered for drug "likeness" by running their proprietary ADME-Tox software to predict log P, log D, water solubility, and Lipinski criteria. The Selector module of Sybyl (Tripos) molecular modeling software was used for structural diversity analysis. The diversity index was 0.01 for a set of 500 compounds. Compounds were sorted and selected using the Unity 2D structural fingerprints built into the software.

Second-generation compounds. The second-generation library was synthesized using a divergent, semiautomated scheme. In the first phase, 4 aromatic aldehydes and phenylacetaldehyde were condensed with 4 hydrophobic primary amines under Borch reductive amination conditions. In the second phase of synthesis, parallel acetylation of these 20 secondary amines with 5 substituted benzoyl chlorides provided the final 100-compound library. A schematic illustration of the strategy used for the synthesis of the second-generation compounds is shown in Supplemental Figure 2. All final products were purified by preparative reverse-phase (C18) HPLC. Compound purity (>95%) was assessed by analytical reverse-phase HPLC and identity verified by mass spectrometry.

Radiolabeling of RAGE ligands. Human Aβ40 and Aβ42 were synthesized at the W. M. Keck Foundation Biotechnology Resource Laboratory (Yale University, New Haven, Connecticut, USA) using solid-phase N-t-butyloxy-carbonyl chemistry and purified by HPLC, as reported (9, 10). Na125I was obtained from NEN Radiochemicals. Radioiodination of Aβ40 and Aβ42 (10 μg) was carried out by the mild lactoperoxidase method using 2 mCi Na125I (9). The monoiodinated nonoxidized forms of Aβ were purified by reverse-phase HPLC and their identity confirmed by MALDI-TOF mass spectrometry, as reported (9, 60). The specific activity of 125I-Aβ peptide was 45 to 65 μCi/μg peptide. Recombinant human amphoterin (HMGB1; R&D Systems) and recombinant human S100B (OriGene Technologies) (10 μg) were radiolabeled using 0.5 mCi Na125I by Iodo-Gen (Thermo Scientific). Free iodide was removed by gel filtration. 125I-labeled ligands had specific activity of approximately 20 μCi/μg. In all studies, radiolabeled ligands were used within 24 hours of labeling.

Aβ binding to RAGE-CHO cells. 125I-Aβ40 (5 nM) binding to cell-surface RAGE in RAGE-transfected CHO cells was performed at 4°C in the presence of different concentrations of unlabeled Aβ40 (10–200 nM), as reported (32). This study was performed to validate the assay that we used later in the primary and secondary screens. We confirmed a saturable nature of Aβ/RAGE binding in RAGE-CHO cells with the binding constant (K_d) of 75 ± 5 nM and maximal binding capacity (B_{max}) of 0.25 ± 0.03 nmoles/h/10^4 cells (Supplemental Figure 1B), which is similar to what has been reported (32). The K_d and B_{max} values were determined using a nonlinear regression analysis software package (GraphPad Prism version 3.02; GraphPad Software).

Screening strategy. The 125I-Aβ40–binding assay in RAGE-CHO cells was performed as reported (32) and described above. First, we incubated RAGE-CHO cells at 4°C for 3 hours with 125I-Aβ40 (5 nM) in the absence or presence of 5,000 small-molecule library compounds used at a concentration of 10 μM. At the end of the incubation period, cells were washed with the cold nonradioactive medium to remove 125I-Aβ40. Cells were then lysed in a solution containing 1% NP-40 in 0.1 M NaCl at 37°C for 15 minutes. Radioactivity was determined using 1470 Wallac Wizard Gamma Counter (PerkinElmer). The fraction of 125I-Aβ40 that was bound to the cell-surface RAGE was determined as previously reported (32). The primary screen revealed 7 compounds out of 5,000 that inhibited Aβ/RAGE binding.

To determine the relative inhibitory affinity of 7 compounds from the primary screen, we next studied their ability to block Aβ/RAGE binding at a much lower concentration of 50 nM, which is close to the K_d value for Aβ binding to RAGE in RAGE-CHO cells (i.e., 75 nM; see above, *A*β binding to RAGE-CHO cells). We used the velocity ratio method to determine the inhibitory constant K_i for each compound, as we have previously reported (9, 52) (see below, Equation 1). Because our goal was to select the highest affinity blockers, we used a stringent criterion, that K_i was not to be greater than $3 \times K_d$ for Aβ/RAGE binding in RAGE-CHO cells. Using this criterion, we identified 3 lead high-affinity blockers out of 7, named FPS1, FPS2, and FPS3. One of these compounds (i.e., FPS2) was a better blocker of 125I-Aβ40 binding to RAGE than unlabeled Aβ itself when studied at comparable equimolar concentrations, i.e., the K_i/K_d ratio was 0.66 (Table 1). The remaining 4 compounds have not been considered for further studies because of their relatively low affinity as Aβ/RAGE inhibitors.

We used the 125I-Aβ40–binding assay in RAGE-CHO cells for the secondary library screen. The second-generation library of 100 compounds was synthesized as explained in Results, with a goal of obtaining a compound with enhanced BBB permeability, but still high affinity, to inhibit Aβ/RAGE binding. Using a stringent criterion, that the K_i of the lead inhibitor should be comparable to FPS2, the secondary screen revealed 1 compound out of 100 (i.e., FPS-ZM1) that satisfied both criteria, i.e., enhanced BBB permeability and high-affinity blockade of Aβ/RAGE binding (Table 1).

The lead compounds from the primary (i.e., FPS2) and secondary (i.e., FPS-ZM1) screen were next tested at different concentrations (i.e., from 10 to 1,000 nM) for their efficacy in inhibiting Aβ/RAGE binding in multiple cell-free and cell-based assays, as described below (see Cell-free assays and Cell-based assays).

The inhibitory constant, K_i. The inhibitory constant (K_i) was determined using Equation 1, as reported (9, 52).

K_i (nM) = $(B_o \times K_d \times C_i)/(B_o – B_i)(K_d + C_{A\beta})$

(Equation 1)

where B_o and B_i are ^{125}I-Aβ binding in the absence and presence of an inhibitor, and C_i and $C_{A\beta}$ are the concentrations in the medium of the inhibitor (50 nM) and ^{125}I-Aβ40 (5 nM), respectively. K_d is the binding constant of Aβ determined in a separate set of studies (see below, Aβ binding to RAGE-CHO cells) and reported before (32).

Cell-free assays

Binding of Aβ and other ligands to sRAGE. Human sRAGE obtained from Bio-Vendor was immobilized (10 μg/ml) overnight at 4°C in 96-well microtiter plates and blocked with 3% bovine serum albumin. ^{125}I-labeled Aβ40, HMGB1, or S100B at 5 nM in the absence and presence of various concentrations of FPS2 or FPS-ZM1 (10 to 1,000 nM) was added to the wells (in triplicate) containing immobilized sRAGE and incubated for 1 hour at room temperature in PBS. Wells were washed with cold PBS to remove unbound radiolabeled ligands, and the radioactivity was analyzed by using the Wallac Wizard Gamma Counter. The effects of RAGE-specific V domain, C1 domain, and C2 domain antibodies (20 μg/ml) (provided by Gunter Fritz) on ^{125}I-Aβ40 (5 nM) binding to immobilized sRAGE were determined in the presence and absence of 100 nM FPS-ZM1. Binding of ^{125}I-ligands to immobilized sRAGE or its recombinant domains in the presence of various potential inhibitors (e.g., FPS2, FPS-ZM1, RAGE antibodies) was expressed as a percentage of control binding of ^{125}I-labeled ligands in the absence of inhibitors that was arbitrarily taken as 100%.

Binding of Aβ to RAGE domains. The recombinant human RAGE V domain and C1–C2 domains (provided by Gunter Fritz) were immobilized (10 μg/ml) overnight at 4°C in 96-well microtiter plates and blocked with 3% bovine serum albumin. ^{125}I-Aβ40 (5 nM) binding to immobilized V domain and C1–C2 domains was determined in the presence and absence of 100 nM FPS-ZM1. Binding of ^{125}I-Aβ40 to RAGE domains in the presence of FPS-ZM1 was expressed as a percentage of control binding of ^{125}I-Aβ40 in the absence of FPS-ZM1 that was arbitrarily taken as 100%.

Binding of Aβ to LRP. Aβ binding to human plasma–derived sLRP in the presence of vehicle (PBS), FPS-ZM1, or RAP was determined using ELISA. Briefly, 10 μg/ml human sLRP was coated on microtiter plates and blocked with protein-free blocking buffer (37570; Pierce). Aβ40 or Aβ42 (100 nM) was added and incubated in HBSC (HEPES-buffered saline containing 5 mM calcium), pH 7.4, for 2 hours at room temperature in the presence of vehicle, FPS-ZM1 (1 μM), or RAP (1 μM). After washing with HBSC containing 0.1% Tween 20, the N-terminal–specific anti-Aβ primary antibody (1 μg/ml; catalog #2454, Cell Signaling) was added and incubated overnight. The secondary antibody for the N-terminal anti-Aβ antibody was HRP-conjugated goat anti-rabbit (1:3000; Dako). The reaction was developed with 3,3′5,5′-tetramethlbenzidine (TMB) (KPL), stopped with 1 N HCl, and the absorbance read at 450 nm.

FPS-ZM1 incubation with immobilized sRAGE or RAGE ligands. To determine whether FPS-ZM1 binds directly to sRAGE or Aβ and other studied RAGE ligands, sRAGE, Aβ40, S100, and HMGB1 were immobilized directly onto an agarose support using a Pierce Direct IP kit (catalog no. 26148) and incubated with equimolar concentration of FPS-ZM1 (200 nM) in PBS for 3 hours at room temperature on a rotary shaker (Glas-Col). At the end of the incubation period, the samples were spun at 12,000 g for 20 seconds,

and the pellet and supernatant used for FPS-ZM1 detection. The pellet containing sRAGE or RAGE ligands was extracted with acetonitrile (60 μl). The supernatant that did not contain sRAGE, Aβ, or RAGE ligands (15 μl) was also extracted with acetonitrile (100 μl), vacuum dried, and resuspended in acetonitrile (60 μl). FPS-ZM1 was detected in all samples (20 μl) by electrospray ionization–liquid chromatography/tandem mass spectrometry (see below, Drug measurements).

Cell-based assays

Cell toxicity assay. To determine whether FPS2 and FPS-ZM1 are toxic to CHO cells, the cells were treated for 72 hours with different concentrations of inhibitors ranging from 10 nM to 10 μM. The cellular toxicity was determined using the WST-8 Assay Kit (Dojindo Molecular Technologies). In this assay, the amount of the water-soluble formazan dye generated is directly proportional to the number of live cells. The WST-8 assay was also used to determine the cell survival of SH-SY5Y cells (see below) after treatment with 1 μM Aβ40 or Aβ42 oligomers and 1 μM Aβ40 or Aβ42 aggregates with or without 1 μM FPS-ZM1 for 24 hours. Aβ40 and Aβ42 oligomers and Aβ40 and Aβ42 aggregates were prepared as previously described (31, 61). Formation of Aβ40 and Aβ42 oligomers and aggregates was confirmed by dot blot analysis using Aβ oligomer–specific A11 and Aβ aggregate–specific OC antibody, respectively (antibodies were provided by Charles Glabe, University of California Irvine, Irvine, California, USA). Cell survival rates of the Aβ oligomer– and Aβ aggregate–treated cells were expressed as the percentages of viable cells compared with vehicle-treated cells.

TBARS. CHO cells were treated with 1 μM Aβ40 with and without various concentrations of FPS2 or FPS-ZM1 for 4 hours. DMSO (0.05%) was used as vehicle. After treatment, cells were collected and lysed in RIPA buffer containing a cocktail of complete protease inhibitors (Roche Diagnostics). A solution containing 0.1 ml of 1.15% KCl, 0.1 ml 8.1% SDS, 0.75 ml 20% acetic acid (pH 3.5), and 0.75 ml 1% aqueous thiobarbituric acid (Sigma-Aldrich) was added to each cell lysate sample (7×10^5 cells). The mixture was then heated at 100°C for 60 minutes in tightly capped tubes. After the samples were cooled down to 25°C, 0.1 ml distilled water was added. TBARS were extracted with 2.5 ml n-butanol:pyridine (15:1; Sigma-Aldrich) and centrifuged (1,000 g; 20 minutes) to separate the organic and aqueous phases and the cell debris. The organic phase was analyzed at 532 nm using a spectrophotometer (UV160U; Shimadzu).

Gel mobility shift assay (NF-κB). CHO cells were treated with and without Aβ40 (1 μM), FPS2, or FPS-ZM1 for 4 hours and nuclear proteins extracted using NE-PER (Pierce). Nuclear proteins (10 μg) were then incubated for 20 minutes at room temperature in 20 ml Tris buffer (5 mM, pH 8.0) containing 0.2 mg/ml poly (DI:dC), 0.5 mM DTT, 0.5 mM EDTA, 25 mM NaCl, 1% Ficoll, and 50 pg/ml digoxigenin-labeled (DIG-labeled) probe. Samples were then loaded on a 4% polyacrylamine 0.25 × TBE gel. The gel was transferred to Hybond N⁺ membrane (Amersham Biosciences) and the DNA/protein complex detected using conjugated streptavidin-HRP. Intensity of the NF-κB blots was determined using AlphaImager 2200 (Alpha Innotech).

Oxidative stress. Oxidative stress in RAGE-CHO cells was determined using 10 μM of 2′-7′-dihydrofluorescein diacetate (DCF) (Invitrogen) after 30 minutes incubation in DMEM (Invitrogen) at 37°C. Fluorescence levels were quantified using a fluorescent reader (Multilabel Counter 1420; PerkinElmer), with excitation at 485 nm and emission at 535 nm. Images were observed and recorded using confocal microscopy (LSM 510 meta; Zeiss).

SH-SY5Y cells. Human neural SH-SY5Y cell line was purchased from ATCC (CRL-2266). The cells were grown in a 1:1 mixture of DMEM and Ham's F12 supplemented with 10% fetal calf serum, 10 U/ml penicillin, and 100 μg/ml streptomycin (Invitrogen), to approximately 75% confluence.

Adenoviruses. The SH-SY5Y cells were transduced at 200 MOI for 6 hours in serum-free medium at 37°C with GFP expressing adenovirus (Ad. GFP) or adenovirus encoding the mutant form of IκB-α (S32, 36A; Ad. IκB-α) provided by Sanjay Maggirwar (University of Rochester, New York, New York, USA). Cells were studied within 48 hours of transduction.

siRNA. SH-SY5Y cells were grown to 75% confluence and washed with PBS. Control or RAGE siRNA mixture in Accell delivery medium to the final concentration of 1 μM was added to the cells. Maximum knockdown efficiency for RAGE was observed 72 hours after transfection. Accell SMARTpool targeted to human RAGE and negative-control Accell nontargeting pool were purchased from Dharmacon. Accell SMARTpool siRNA for human RAGE comprised 4 target siRNAs, i.e., CCCUGGUGCCUAAUGAGAA, GGAGUAUCUGUGAAGGAAC, GGAGCGUGCAGAACUGAAU, and CUCUUAGCUGGCACUUGGA. Cells were transfected using Accell delivery medium (Dharmacon) according to the manufacturer's instructions.

Quantitative RT-PCR. Total RNA from SH-SY5Y cells was isolated using the RNeasy kit (QIAGEN). cDNA was prepared from RNA using the iScript cDNA synthesis kit (Bio-Rad). The real-time PCR amplification was performed by SYBR green method on a Bio-Rad iCycler iQ Real-Time PCR Detection System, using iQ SYBR Green Supermix (Bio-Rad) as a fluorescent DNA interacting agent. The following primers were used: human *BACE1*, sense, TGGAGGGCTTCTACGTTGTCTT, anti-sense, CCTGAACTCATCGTGCACATG; mouse *Bace1*, sense, GATGGTGGACAACCTGAG, anti-sense, CTGGTAGTAGCGATGCAG; mouse *Tnfα*, sense, 5′-GACAAGGCTGCCCCGACTA-3′, anti-sense, 5′-TTTCTCCTGGTATGAGATAGCAAATC-3′; mouse *Il1β*, sense, 5′-TCGCTCAGGGTCACAAGAAA-3′, anti-sense, 5′-ATCAGAGGCAAGGAGGAAACAC-3′; mouse *Il6*, sense, 5′-TGGAGTCACAGAAGGAGTGGCTAAG-3′, anti-sense, 5′-TCTGACCACAGTGAGGAATGTCCAC-3′; mouse *Ccl2*, sense, 5′-GGCTCAGCCAGATGCAGTTAA-3′, anti-sense, 5′-CCTACTCATTGGGATCATCTTGCT-3′; human *GAPDH*, sense, 5′-CCACCCATGGCAAATTCCATGGCA-3′, anti-sense, 5′-TCTAGACGGCAGGTCAGGTCCACC-3′; and mouse *Gapdh*, sense, 5′-ACCACAGTCCATGCCATCAC-3′, anti-sense, 5′-TCCACCACCCTGTTGCTGTA-3′. Normalization of cDNA levels was performed with glyceraldehyde 3-phosphate dehydrogenase for each template and final abundance adjusted to yield an arbitrary value of 100 for control templates using the ΔΔCt method. Levels of mRNA were expressed as a percentage of control.

Western blot analysis. CHO and SH-SY5Y cells were prepared in RIPA lysis buffer containing a cocktail of complete protease inhibitors (Roche Diagnostics) and lithium dodecyl sulfate sample buffer (Invitrogen). Proteins were separated by electrophoresis on NuPAGE Novex Bis-Tris (Bis [2-hydroxyethyl] imino-tris [hydroxymethyl] methane-HCl) precast 4% to 12% gradient gels (Invitrogen). The separated proteins were transferred on nitrocellulose membrane, and the membranes were blocked with 5% nonfat milk (Bio-Rad) in Tris-buffered saline containing 0.1% Tween 20 (TBST) for 1 hour at room temperature. The membranes were then probed overnight at 4°C with primary rabbit polyclonal anti-BACE1 antibody (1:1000; Abcam) and incubated with HRP-conjugated secondary goat anti-rabbit antibody (1:5000; Santa Cruz Biotechnology Inc.) for 1 hour at room temperature. Goat anti–β-actin antibody (1:5000; Santa Cruz Biotechnology Inc.) and donkey anti-goat antibody (1:7000) were used to detect β-actin. For detection of RAGE, we used primary goat anti-RAGE antibody (1:2000; R&D Systems) and HRP-conjugated donkey anti-goat antibody (1:7000; Santa Cruz Biotechnology Inc.) as a secondary antibody. Membranes were washed in TBST and incubated for 5 minutes with SuperSignal West Pico Chemiluminescent Substrate (Pierce), exposed to CL-XPosure film (Pierce) and developed in a X-OMAT 3000 RA film processor (Kodak). Blots were imaged using

AlphaImager 2200 (Alpha Innotech), and densitometry analysis was performed using Alpha Ease FC software (Alpha Innotech). The signal intensity of protein bands was normalized to β-actin.

sAPPβ. The levels of sAPPβ in the medium from cultured SH-SY5Y cells were determined using an ELISA kit (Covance).

BV-2 cell line. The immortalized murine microglial (BV-2) cells were provided by Sanjay Maggirwar. The cells were grown to 75%–85% confluence in DMEM supplemented with 10% FBS, 100 U/ml penicillin G, and 0.1 mg/ml of streptomycin (Invitrogen) at 37°C and 5% CO_2. The cells were next treated with Aβ40 (1 μM) for 24 hours in the absence and presence of FPS-ZM1 (50 nM). Cells were also transduced with adenoviruses encoding GFP or the mutant form of IκB-α (S32, 36A), as described previously. The conditioned medium was analyzed immediately to determine the levels of secreted TNF-α and IL-1β using Quantikine mouse TNF-α and IL-1β ELISA kits (R&D Systems). Nuclear extracts were analyzed for NF-κB activation by using gel shift assay, as described above, or for mRNA levels of proinflammatory cytokines by using quantitative RT-PCR (qRT-PCR), as described above. For RAGE expression, cells were fixed in 4% PFA, blocked with 5% swine serum for 1 hour, and incubated with primary goat anti-RAGE antibody (1:200; R&D Systems) overnight at 4°C followed by incubation with donkey anti-goat Cy3 (1:100; Jackson ImmunoResearch) as a secondary antibody. The sections were analyzed by using a Zeiss LSM 510 meta confocal laser scanning microscope equipped with a 40×/1.2 Korr water immersion objective and Zeiss AIM 4.2 software (Carl Zeiss Microimaging).

Studies in wild-type mice

Toxicity studies. FPS2 and FPS-ZM1 were administered at 500 mg/kg i.p. to 2-month-old C57BL/6 mice. This dose was 500 times greater than the daily therapeutic dose given to *APP*[sw/0] mice (see below). Controls were injected with vehicle. Physiological parameters including mean arterial BP, heart rate, blood gasses, respiration rate, and glucose levels were determined before and within 1 hour of drug injection. Mice were observed daily for 7 days for adverse reactions. Body weight was measured before the treatment and at the end of the treatment. Clinical chemistry (hepatic and renal functional tests), organ weight, gross necropsy, and histopathology were performed at the end of the study. Hepatic (code 60405) and renal (code 60406) functional tests were outsourced to Idexx Reference Laboratories. Mean arterial BP and heart rate were monitored via the cannulated right femoral artery using a pressure transducer (MP150; BIOPAC Systems). Blood gases and pH were determined from a small sample (~90 μl) of arterial blood collected from the cannulated right femoral artery, using the Radiometer ABL 77. Respiration rate was recorded using BIOPAC Systems.

BBB permeability to drugs. Briefly, C57BL/6 mice (2 to 3 months old) were anesthetized with ketamine (100 mg/kg) and xylazine (10 mg/kg) and the right femoral artery and vein cannulated. FPS2 or FPS-ZM1 were administered i.v. (1 mg/kg) via the femoral vein and arterial blood samples (30 μl) collected at 1, 5, 10, 15, and 20 minutes via the cannulated femoral artery. Plasma was separated by centrifugation at 4°C and immediately stored at –80°C until analysis. At the terminal time point, the brain was isolated and pial vessels and choroid plexus removed before storing at –80°C. Brain was homogenized in 1:2 (w/v) methanol/water (75:25) by sonication (Mesonix Sonicator 3000). Homogenized brain or plasma (15 μl) was deproteinized with acetonitrile (100 μl), vacuum dried, and resuspended in 20 μl acetonitrile. The levels of FPS2 and FPS-ZM1 in plasma and brain samples were determined by electrospray ionization–liquid chromatography/tandem mass spectrometry as described below (see below, Drug measurements). The permeability surface area (PS) product was determined for both FPS2 and FPS-ZM1 as an acceptable measure of BBB permeability (23) (see below, Calculation of PS product).

BBB permeability to sucrose. C57BL/6 mice (2 to 3 months old) were anesthetized and the right femoral artery and vein cannulated, as above. ^{14}C-sucrose was obtained from GE Healthcare. ^{14}C-sucrose (5 μCi) was administered i.v. and arterial blood (20 μl) collected at 1, 2.5, 5, 7.5, 10, 15, and 20 minutes. Plasma and brain samples were prepared for radioactivity determination. ^{14}C samples were solubilized in 0.5 ml aqueous-based tissue solubilizer (Solvable; PerkinElmer) overnight, followed by addition of 5 ml of scintillation cocktail (Ultima Gold; PerkinElmer) and analysis using a liquid scintillation counter (Tri-Carb 2100TR; Packard Instrument Company). The PS product for ^{14}C-sucrose was determined as described below (see Calculation of PS product).

Calculation of PS product. The BBB permeability to FPS2, FPS-ZM1, and ^{14}C-sucrose was determined as the PS product (μl/g/minute) using Equation 2, as reported (62).

$$C_b = PS \times AUC_{0-T}$$

(Equation 2)

where C_b is the brain concentration of FPS2 or FPS-ZM1 or ^{14}C-sucrose radioactivity (dpm/g brain), and AUC_{0-T} (area under the curve) is the integrated plasma concentration from time 0 to time T (i.e., 20 minutes). Correction for the cerebral intravascular concentration of FPS2 and FPS-ZM1 or ^{14}C-sucrose radioactivity was not needed, since their plasma levels were undetectable at the terminal time point.

Brain uptake of drugs and sucrose. Brain uptake of FPS2 and FPS-ZM1 and ^{14}C-sucrose was expressed as a percentage of their respective integrated plasma concentrations from time 0 to time T (20 minutes).

APP$^{sw/0}$ mice

APP$^{sw/0}$ mice that overexpress human APP transgene with the K670M/N671L double-mutation under control of the hamster prion promoter (36) were obtained from Taconic Farms. Mice were housed under standard conditions (12-hour light/ 12-hour dark cycle starting at 6:30 am; 21 ± 2°C; 55 ± 10% humidity) in solid-bottomed cages on wood chip bedding. We studied the effects of RAGE inhibitors on Aβ BBB transport and Aβ pathology and functional outcome in male *APP$^{sw/0}$* mice, as described in sections below.

Aβ BBB transport in APP$^{sw/0}$ mice

Brain arterial infusion technique. This previously described technique in mice (10, 43) was used to determine the effects of RAGE inhibitors on Aβ transport across the BBB in 15-month-old *APP$^{sw/0}$* mice. Briefly, mice were anesthetized with ketamine (100 mg/kg) and xylazine (10 mg/kg). The right common carotid artery was isolated and cannulated with polyethylene tubing (PE10) connected to an extracorporeal perfusion circuit. The arterial inflow perfusion medium (i.e., mock blood) containing radiolabeled Aβ (see below) was infused into the mouse brain through the common carotid artery at a rate of 1.0 ml/minute using a peristaltic pump (Rainin Instrument). The infusion medium consisted of sheep red blood cells suspended in an artificial plasma solution. For details regarding this technique, including composition of the perfusion medium and control of physiological parameters during these short-term brain arterial infusions, please see LaRue et al. (43). The infusion was terminated by decapitating the animal at predetermined times. The hemisphere ipsilateral to brain arterial perfusion was prepared for radioactivity analysis, as reported (10, 43), and described below.

Influx of ^{125}I-Aβ. We studied Aβ transport across the BBB using brain arterial infusion technique, as described above. Briefly, ^{125}I-Aβ40 at a final concentration of 1.5 nM in the cerebral arterial inflow, corresponding to Aβ levels normally found in plasma of 15- to 17-month-old *APP$^{sw/0}$* mice, was infused through the right common carotid artery of 15-month-old *APP$^{sw/0}$* mice simultaneously with ^{14}C-inulin (NEN Radiochemicals), a cerebro-

vascular space marker, by a slow-drive syringe pump (Harvard Apparatus) at a rate of 0.1 ml/min. The effect of a RAGE antibody (RAGE antibody AF1179, 40 μg/ml; R&D Systems), NI IgG (40 μg/ml), or FPS2 or FPS-ZM1 (200 nM) was studied over 5 minutes of infusion, which was within the linear range of Aβ transport (influx) into the brain, as described (10). The concentrations of FPS2 and FPS-ZM1 used in the cerebral arterial inflow corresponded to an integrated arterial plasma concentration obtained within 20 minutes of an i.p. administration of FPS-2 or FPS-ZM1 at a daily therapeutic dose of 1 mg/kg in *APP$^{sw/0}$* mice.

To confirm that preabsorption of FPS-ZM1 on sRAGE, but not sLRP, results in loss of FPS-ZM1 inhibition of Aβ transport in vivo, we preincubated FPS-ZM1 with immobilized sRAGE or sLRP and tested the effects of the supernatants on Aβ transport into the brain, as described above. Briefly, human sRAGE or sLRP (a recombinant sLRP ligand-binding domain IV, sLRP-IV; MW = 64 kDa; provided by ZZ Alztech LLC) was immobilized onto an agarose support using a Pierce Direct IP kit (cat. no. 26148) and incubated with FPS-ZM1 in PBS for 3 hours at room temperature on a rotary shaker (Glas-Col). At the end of the incubation period, the samples were spun at 12,000 g for 20 seconds and the supernatant removed and tested in Aβ influx studies.

Calculations. ^{125}I-Aβ40 influx into the brain corrected for distribution of ^{14}C-inulin (a cerebrovascular space reference marker) was calculated using Equation 3.

$$\text{Influx} = (V_d/T) \times C_{pl}$$

(Equation 3)

where V_d is the distribution volume of ^{125}I-Aβ40, T is the perfusion time (s), and C_{pl} is the TCA-precipitable ^{125}I-Aβ40 radioactivity in the arterial inflow. $V_d = [(\text{TCA-precipitable } ^{125}\text{I cpm/g brain})/(\text{TCA-precipitable } ^{125}\text{I cpm/ml arterial plasma inflow})] - [(^{14}\text{C dpm/g brain})/(^{14}\text{C dpm/ml of arterial plasma inflow})]$. ^{125}I-Aβ40 influx was expressed in fmol/min/g interstitial fluid (ISF), assuming an ISF volume of 0.1 ml ISF/g brain (10).

FPS-ZM1 binding to RAGE in brain of APP$^{sw/0}$ mice

APP$^{sw/0}$ mice (15 to 17 months old) were anesthetized with ketamine (100 mg/kg) and xylazine (10 mg/kg) i.p. FPS-ZM1 was administered i.v. (1 mg/kg) and after 5 minutes, 6-, 12-, and 24-hour mice were sacrificed. Brain was removed rapidly and immediately stored at –80°C. Brain (50 mg) was homogenized in 10× (w/v) IP assay buffer (Roche Diagnostics) by sonication (Mesonix Sonicator 3000) and centrifuged at 20,000 g for 20 minutes at 4°C. The supernatant was used to IP RAGE using a protein G IP kit (Roche Diagnostic) and RAGE cytoplasmic domain-specific antibody (Abcam) (rabbit anti-human, which cross-reacts with mouse RAGE). FPS-ZM1 in the RAGE-IP fraction was extracted with acetonitrile (60 μl). The RAGE-depleted brain fraction (15 μl) was deproteinized with acetonitrile (100 μl), vacuum dried, and resuspended in acetonitrile (60 μl). In all samples (20 μl), FPS-ZM1 was detected by electrospray ionization–liquid chromatography/tandem mass spectrometry, as described below.

Therapy with RAGE blockers

Treatment of APP$^{sw/0}$ mice. Male *APP$^{sw/0}$* mice were treated with FPS2 or FPS-ZM1 (1 mg/kg/d, i.p.), or vehicle (0.05% DMSO in saline, i.p.) for 2 months starting at 8 or 15 months of age. After 2 months of treatment, we studied functional parameters and determined the CBF response to brain activation (whisker stimulation) and the scores on behavioral tests including NOL, NOR, and operant learning. After functional tests were completed, mice were anesthetized with ketamine (100 mg/kg) and xylazine (10 mg/kg) and transcardially perfused with ice-cold heparinized saline; brains were harvested and hemi-dissected. One hemisphere was embedded in cold OCT embedding medium (Tissue-Tek; Sakura Finetek) on dry

ice for histological studies. Cortex and hippocampus from the opposite hemisphere were dissected, rapidly frozen on dry ice, and stored at –80°C for biochemical studies.

CBF response to whisker stimulation. We measured the CBF responses to vibrissal stimulation in *APP$^{sw/0}$* mice using laser Doppler flowmetry (BLF 21D; Transonic Systems), as described (63). Briefly, mice were anesthetized i.p. with a mixture of urethane (800 mg/kg) and chloralose (50 mg/kg). The tip of the laser Doppler probe was stereotaxically placed 0.5 mm above skull over the whisker barrel area. The right vibrissae were cut to about 5 mm and stimulated by gentle stroking at 3–4 Hz for 1 minute with a cotton-tip applicator followed by a 10-minute recovery period. Three trials were conducted using this procedure. Rectal temperature was maintained at 37°C using a heated blanket (Homeothermic Blanket; Harvard Apparatus). The percentage increase in CBF due to vibrissal stimulation was obtained from the baseline values and averaged for the 3 trials.

NOL and NOR. NOL, a spatial memory hippocampus-dependent test (64), and NOR, a perirhinal cortex-dependent test (65), were performed as we previously described (8, 63). The time exploring the novel and familiar objects was scored to provide a discrimination index, as reported (63).

Operant response. Custom-made mouse operant chambers were used to test response acquisition, as previously described (63). The chambers (130 × 95 × 130 mm) were equipped with a photobeam over an access hole (25 mm) to a liquid reward (evaporated milk) dipper to detect entry. On the opposite side of the chamber, there were 2 "response" holes (15 mm), one "active" and another "inactive," with photobeams to record "pokes" by a mouse's snout. An active operant response was recorded when the mouse poked its snout into an active response hole, moved to the opposite side of the chamber, and entered the dipper hole. Each response hole had a light-emitting diode (LED). The LEDs were turned on during the session and turned off when the photobeam was broken (i.e., feedback stimulus). Each chamber was equipped with a 28-volt incandescent house light that was used to signal the start and end of a session. All data were recorded in real time by a PC. Operant training consisted of 3 sessions (25 minutes) in which rewards were presented on a variable time 60 second (VT60) schedule concomitantly with a fixed ratio 1 (FR1) schedule for snout entries into the active response hole. Mice could wait for the VT60 schedule and receive about 25 milk presentations; active response hole pokes could present milk up to 999 times (programmed limit).

Human Aβ40- and Aβ42-specific ELISA. Hippocampus and cortex were homogenized in ice-cold guanidine buffer (5 M guanidine hydrochloride/50 mM TrisCl, pH 8.0) and used for human Aβ40 and Aβ42 determinations, as described (63). Briefly, Aβ40 and Aβ42 levels in the hippocampus and cortex were determined by using human-specific ELISA kits (Invitrogen) according to the manufacturer's instructions. For human Aβ40 and Aβ42 ELISA, a monoclonal antibody specific against the NH$_2$ terminus of human Aβ was used as the capturing antibody and a rabbit antibody specific for the COOH-terminus of either Aβ40 or Aβ42 was used as the detecting antibody.

Aβ immunostaining. Acetone-fixed cryostat brain slices (10 μm) were treated with 70% formic acid, blocked with PBS containing 5% swine serum, and incubated with human-specific rabbit anti-Aβ (Invitrogen). Next, the sections were incubated with fluorescein-conjugated donkey anti-rabbit IgG (Invitrogen). Quantification of total Aβ load in the cortex and hippocampus was performed in 4 groups of tissue sections, each separated by 200 μm and each containing three 10-μm sections, using Image-Pro Plus Software (Media Cybernetics), as previously described (63).

Amyloid deposits. Acetone-fixed cryostat brain tissue sections (10 μm) were stained with a filtered 1% thioflavin S (Sigma-Aldrich) solution in 70% ethanol, as described (63). The total area of amyloid-associated thioflavin S deposits was determined as a percentage of total brain section area using Image-Pro Plus Software (Media Cybernetics). In some studies, we performed staining with 10 μM methoxy X-04 (Neuroptix) in 40% ethanol and then sequentially washed with 40% ethanol, 90% ethanol, and ddH$_2$O. Following staining with methoxy X-04, the sections were immunostained with Iba1, as described below.

Microglia. Formaldehyde-fixed brain sections (40 μm) were used to immunostain microglia for ionized calcium-binding adaptor molecule 1 (Iba1). Sections were permeabilized with 0.4% Triton X-100 in PBS, blocked with 5% swine serum for 1 hour, incubated with the primary antibody goat anti-Iba1 (1:200; Abcam) overnight at 4°C, and washed with 0.1% Triton X-100 in PBS; Iba1 was detected with secondary antibody donkey anti-goat DyLight 488 nm (1:150; Jackson ImmunoResearch) after incubation at room temperature for 1 hour. Amyloid plaques were stained with methoxy-XO4 as described above. The sections were then washed 3 times with PBS. The slides were mounted with Dako mounting medium (Dako) and imaged using an upright Zeiss LSM 510 meta confocal laser scanning microscope equipped with a 40×/1.2 Korr water immersion objective, an Argon laser line of 488 nm, 543 nm HeNe, and 633 nm HeNe, 800 nm Ti:sapphire (Mai Tai; Spectra Physics), and Zeiss AIM 4.2 software (Carl Zeiss Microimaging). Images were processed using Zeiss Zen 2007 Light Edition software (Carl Zeiss Microimaging). The number of Iba1-positive microglia from 4 mice per group in the cortex was counted from 7 nonadjacent sections (approximately 100 μM apart) per mouse. Images were taken from cortex in 1 plane and cells counted using ImageJ software (Media Cybernetics) with cell counter plug-in analysis tool. However, to show the accumulation of microglia around plaques, images were taken from 40-μm–thick sections at different planes and merged as Z-projection.

Laser capture microdissection. Mouse brains were snap-frozen, cut (10 μm) using Microm HM 500M cryostat (Thermo Fisher), and mounted on RNase-free PALM membrane slides (Carl Zeiss Microimaging). The sections were fixed with ice-cold acetone for 5 minutes and stained using goat anti-Iba1 (microglia, 1:150) or mouse anti-neuronal nuclei (NeuN, 1:200; Abcam) antibodies. The secondary antibodies were HRP-conjugated rabbit anti-goat and goat anti-mouse (1:50; Dako). Positive staining was detected by a brief incubation in 3-3′-diaminobenzidine (DAB). The stained cells were captured on laser capture microdissection (LCM) caps using contaminated–free LCM on dried sections at 400 magnification with a Zeiss Axiovert 200 inverted microscope equipped with 337 nm laser and robotic microscope table operated by PalmRobo software (Carl Zeiss Microimaging). Stained microglia and neurons were randomly chosen from 8–10 sections per mouse for 4 mice per group. Approximately 1,000 cells were captured per sample and stored at –80°C until required for RNA isolation.

qRT-PCR. The mRNA levels for *Bace1*, *Tnfα*, *IL1β*, *IL6*, and *Ccl2* in snap-frozen brain sections as well as laser-captured microglia and neurons from the cortex and hippocampus were determined using primers as described above for qRT-PCR (see Cell-based assays).

Western blot analysis. BACE1 protein levels were determined in mouse brain tissue using BACE1-specific antibodies and β-actin as a loading control as described above for Western blot analysis (see Cell-based assays).

sAPP-β, TNF-α, and IL-1β by ELISA. The cortex and hippocampus were snap-frozen and homogenized with pellet pestle in complete lysis-M buffer containing protease inhibitors (Roche Diagnostics). Lysates were further homogenized by sonication (Mesonix Sonicator 3000) using 5 pulses of 30 seconds each on ice. The homogenate was agitated on ice for 30 minutes and then centrifuged at 4°C and 15,000 *g* for 20 minutes. Supernatant was

immediately used to determine the levels of sAPPβ using the ELISA Kit (Covance). Supernatant was also used to determine levels of TNF-α and IL-1β using the Quantikine Mouse ELISA Kit (R&D Systems).

Detection of active NF-κB. Nuclear-activated NF-κB was determined in brain nuclear extracts similarly to what was previously reported (45) by using the p65 Transcription Factor Kit (Thermo Scientific). The nuclear fraction was extracted using NE-PER nuclear extraction reagents (Thermo Scientific) prepared in RIPA lysis buffer and immediately assayed for nuclear-activated NF-κB using NF-κB consensus sequence and following the manufacturer's protocol.

Oxidative stress. Unfixed brain sections were stained with 1 μM of dihydroethidine hydrochloride (DHE) (Invitrogen) and Alexa Fluor 488–conjugated anti-NeuN antibody (1:150; Millipore), as reported (66). Images were taken immediately using an upright Zeiss LSM 510 meta confocal laser-scanning microscope and Zeiss AIM 4.2 software (Carl Zeiss Microimaging). The quantification of the oxidative stress levels was done with Image-Pro Plus software (Media Cybernetics).

Drug measurements

FPS2 and FPS-ZM1 were detected in different samples by electrospray ionization–liquid chromatography/tandem mass spectrometry, similarly to what was reported previously (67). Briefly, the chromatography was carried out on a Prominence UFLC (Shimadzu) using a 30 mm × 2.1 mm BDS hypersil C18 column (3 micron) fitted with a hyper-select gold C18-RP (5 micron) guard column, 10 mm × 2 mm. A binary linear gradient elution with water (0.1 % formic acid; solvent A) and acetonitrile (0.1 % formic acid; solvent B) was used at a flow rate of 0.5 μl/min. The following program was used: the initial composition was 85% solvent A for about 1 minute, followed by 95% solvent B over 8–9 minutes, and then 85% solvent A at 9.1 minutes until the end of run at 12 minutes.

The mass spectrometer, TSQ Ultra (Thermo Fisher), was operated in the positive ion mode using electrospray ionization. With a capillary temperature of 250°C, the collision gas (nitrogen) pressure was a constant 1.0 mTorr, and the collision energy was set at 25 eV. The SRM transitions monitored for the respective purified internal standards were as follows: for FPS2, m/z 548 to m/z 188 with a collision energy set at 19; for FPS-ZM1, m/z 327 to m/z 240 with a collision energy of 15. The resolution of the first and third quadrupole, FWHM, was set at 0.7 amu.

Statistics

All values were expressed as mean ± SEM. Comparison of parameters among 2 groups was made by Student's t test. Comparison of parameters among more than 2 groups was made by 1-way ANOVA followed by post hoc analysis using Tukey test. For the operant response, statistical analyses were performed using SYSTAT 10 software (Systat Software).The differences were considered to be significant at $P < 0.05$.

Study approval

All studies were performed according to NIH guidelines using protocols approved by the University of Rochester Committee on Animal Resources.

Address correspondence to: Berislav V. Zlokovic, Center for Neurodegeneration and Regeneration, The Zilkha Neurogenetic Institute, Keck School of Medicine, University of Southern California, 1501 San Pablo St., Los Angeles, California 90089, USA. Phone: 585.273.3131; Fax: 585.273.3133; E-mail: berislav_zlokovic@urmc.rochester.edu.

1. Querfurth HW, LaFerla FM. Alzheimer's disease. *N Engl J Med.* 2010;362(4):329–344.
2. Hardy J, Selkoe DJ. The amyloid hypothesis of Alzheimer's disease: progress and problems on the road to therapeutics. *Science.* 2002; 297(5580):353–356.
3. Cummings JL. Alzheimer's disease. *N Engl J Med.* 2004;351(1):56–67.
4. Zlokovic BV. Neurovascular mechanisms of Alzheimer's neurodegeneration. *Trends Neurosci.* 2005;28(4):202–208.
5. de la Torre JC. Vascular risk factor detection and control may prevent Alzheimer's disease. *Ageing Res Rev.* 2010;9(3):218–225.
6. Marchesi VT. Alzheimer's dementia begins as a disease of small blood vessels, damaged by oxidative-induced inflammation and dysregulated amyloid metabolism: implications for early detection and therapy. *FASEB J.* 2011;25(1):5–13.
7. Zlokovic BV. Neurovascular pathways to neurodegeneration in Alzheimer's disease and other disorders. *Nat Rev Neurosci.* 2011;12(12):723–738.
8. Bell RD, et al. Pericytes control key neurovascular functions and neuronal phenotype in the adult brain and during brain aging. *Neuron.* 2010;68(3):409–427.
9. Deane R, et al. LRP/amyloid beta-peptide interaction mediates differential brain efflux of Abeta isoforms. *Neuron.* 2004;43(3):333–344.
10. Deane R, et al. RAGE mediates amyloid-beta peptide transport across the blood-brain barrier and accumulation in brain. *Nat Med.* 2003;9(7):907–913.
11. Eisele YS, et al. Peripherally applied Abeta-containing inoculates induce cerebral beta-amyloidosis.

Science. 2010;330(6006):980–982.
12. Atwood CS, Bishop GM, Perry G, Smith MA. Amyloid–beta: a vascular sealant that protects against hemorrhage? *J Neurosci Res.* 2002;70(3):356.
13. Kumar-Singh S, et al. Dense-core plaques in Tg2576 and PSAPP mouse models of Alzheimer's disease are centered on vessel walls. *Am J Pathol.* 2005;167(2):527–543.
14. Cullen KM, Kocsi Z, Stone J. Microvascular pathology in the aging human brain: evidence that senile plaques are sites of microhaemorrhages. *Neurobiol Aging.* 2006;27(12):1786–1796.
15. Weller RO, Subash M, Preston SD, Mazanti I, Carare RO. Perivascular drainage of amyloid-beta peptides from the brain and its failure in cerebral amyloid angiopathy and Alzheimer's disease. *Brain Pathol.* 2008;18(2):253–266.
16. Bell RD, et al. SRF and myocardin regulate LRP-mediated amyloid-beta clearance in brain vascular cells. *Nat Cell Biol.* 2009;11(2):143–153.
17. Yan SD, et al. RAGE and amyloid-beta peptide neurotoxicity in Alzheimer's disease. *Nature.* 1996;382(6593):685–691.
18. Walsh DM, et al. Naturally secreted oligomers of amyloid beta protein potently inhibit hippocampal long-term potentiation in vivo. *Nature.* 2002;416(6880):535–539.
19. Takuma K, et al. RAGE-mediated signaling contributes to intraneuronal transport of amyloid-beta and neuronal dysfunction. *Proc Natl Acad Sci U S A.* 2009;106(47):20021–20026.
20. Meyer-Luehmann M, et al. Exogenous induction of cerebral beta-amyloidogenesis is governed by agent and host. *Science.* 2006;313(5794):1781–1784.

21. Meyer-Luehmann M, et al. Rapid appearance and local toxicity of amyloid-beta plaques in a mouse model of Alzheimer's disease. *Nature.* 2008;451(7179):720–724.
22. Prusiner SB. *Prion Biology and Diseases.* Vol. 41. Woodbury, New York, USA: Cold Spring Harbor Laboratory Press; 2004.
23. Zlokovic BV. The blood-brain barrier in health and chronic neurodegenerative disorders. *Neuron.* 2008;57(2):178–201.
24. Neeper M, et al. Cloning and expression of a cell surface receptor for advanced glycosylation end products of proteins. *J Biol Chem.* 1992; 267(21):14998–15004.
25. Yan SF, Ramasamy R, Schmidt AM. The RAGE axis: a fundamental mechanism signaling danger to the vulnerable vasculature. *Circ Res.* 2010; 106(5):842–853.
26. Park H, Boyington JC. The 1.5 A crystal structure of human receptor for advanced glycation end-products (RAGE) ectodomains reveals unique features determining ligand binding. *J Biol Chem.* 2010;285(52):40762–40770.
27. Koch M, et al. Structural basis for ligand recognition and activation of RAGE. *Structure.* 2010;18(10):1342–1352.
28. Bucciarelli LG, et al. RAGE blockade stabilizes established atherosclerosis in diabetic apolipoprotein E-null mice. *Circulation.* 2002;106(22):2827–2835.
29. Bierhaus A, et al. Understanding RAGE, the receptor for advanced glycation end products. *J Mol Med.* 2005;83(11):876–886.
30. Schmidt AM, Sahagan B, Nelson RB, Selmer J, Rothlein R, Bell JM. The role of RAGE in amyloid-beta

peptide-mediated pathology in Alzheimer's disease. *Curr Opin Investig Drugs.* 2009;10(7):672–680.

31. Sturchler E, Galichet A, Weibel M, Leclerc E, Heizmann CW. Site-specific blockade of RAGE-Vd prevents amyloid-beta oligomer neurotoxicity. *J Neurosci.* 2008;28(20):5149–5158.

32. Mackic JB, et al. Human blood-brain barrier receptors for Alzheimer's amyloid-beta 1- 40. Asymmetrical binding, endocytosis, and transcytosis at the apical side of brain microvascular endothelial cell monolayer. *J Clin Invest.* 1998;102(4):734–743.

33. Giri R, et al. beta-amyloid-induced migration of monocytes across human brain endothelial cells involves RAGE and PECAM-1. *Am J Physiol Cell Physiol.* 2000;279(6):C1772–C1781.

34. Yan SD, et al. Non-enzymatically glycated tau in Alzheimer's disease induces neuronal oxidant stress resulting in cytokine gene expression and release of amyloid beta-peptide. *Nat Med.* 1995;1(7):693–699.

35. RI: RAGE inhibitor study. Alzheimer's Disease Education and Referral Center. NIH National Institute on Aging Web site. http://www.alzheimers.org/clinicaltrials/fullrec.asp?PrimaryKey=287. Accessed February 14, 2012.

36. Hsiao K, et al. Correlative memory deficits, Abeta elevation, and amyloid plaques in transgenic mice. *Science.* 1996;274(5284):99–102.

37. van de Waterbeemd H, Camenisch G, Folkers G, Chretien JR, Raevsky OA. Estimation of blood-brain barrier crossing of drugs using molecular size and shape, and H-bonding descriptors. *J Drug Target.* 1998;6(2):151–165.

38. Andrews PR, Craik DJ, Martin JL. Functional group contributions to drug-receptor interactions. *J Med Chem.* 1984;27(12):1648–1657.

39. Paris D, et al. Inhibition of Abeta production by NF-kappaB inhibitors. *Neurosci Lett.* 2007; 415(1):11–16.

40. Bourne KZ, Ferrari DC, Lange-Dohna C, Rossner S, Wood TG, Perez-Polo JR. Differential regulation of BACE1 promoter activity by nuclear factor-kappaB in neurons and glia upon exposure to beta-amyloid peptides. *J Neurosci Res.* 2007;85(6):1194–1204.

41. Guglielmotto M, et al. AGEs/RAGE complex upregulates BACE1 via NF-kappaB pathway activation. *Neurobiol Aging.* 2012;33(1):196.e13–e27.

42. LaFerla FM, Green KN, Oddo S. Intracellular amyloid-beta in Alzheimer's disease. *Nat Rev Neurosci.* 2007;8(7):499–509.

43. LaRue B, et al. Method for measurement of the blood–brain barrier permeability in the perfused mouse brain: application to amyloid–beta peptide in wild type and Alzheimer's Tg2576 mice. *J Neurosci Methods.* 2004;138(1–2):233–242.

44. Pfeifer M, et al. Cerebral hemorrhage after passive anti-Abeta immunotherapy. *Science.* 2002;298(5597):1379.

45. Sung S, et al. Modulation of nuclear factor-kappa B activity by indomethacin influences A beta levels but not A beta precursor protein metabolism in a model of Alzheimer's disease. *Am J Pathol.* 2004;165(6):2197–2206.

46. Lue LF, et al. Involvement of microglial receptor for advanced glycation endproducts (RAGE) in Alzheimer's disease: identification of a cellular activation mechanism. *Exp Neurol.* 2001;171(1):29–45.

47. Mann GE, Zlokovic BV, Yudilevich DL. Evidence for a lactate transport system in the sarcolemmal membrane of the perfused rabbit heart: kinetics of unidirectional influx, carrier specificity and effects of glucagon. *Biochim Biophys Acta.* 1985;819(2):241–248.

48. Zlokovic BV, Apuzzo ML. Cellular and molecular neurosurgery: pathways from concept to reality--part I: target disorders and concept approaches to gene therapy of the central nervous system. *Neurosurgery.* 1997;40(4):789–803

49. Zlokovic BV, Begley DJ, Chain-Eliash DG. Blood-brain barrier permeability to leucine-enkephalin, D-alanine2-D-leucine5-enkephalin and their N-terminal amino acid (tyrosine). *Brain Res.* 1985;336(1):125–132.

50. Zlokovic BV, Segal MB, Begley DJ, Davson H, Rakic L. Permeability of the blood–cerebrospinal fluid and blood–brain barriers to thyrotropin–releasing hormone. *Brain Res.* 1985;358(1–2):191–199.

51. Zlokovic BV, Mackic JB, Djuricic B, Davson H. Kinetic analysis of leucine-enkephalin cellular uptake at the luminal side of the blood-brain barrier of an in situ perfused guinea-pig brain. *J Neurochem.* 1989;53(5):1333–1340.

52. Zlokovic BV, Hyman S, McComb JG, Lipovac MN, Tang G, Davson H. Kinetics of arginine-vasopressin uptake at the blood-brain barrier. *Biochim Biophys Acta.* 1990;1025(2):191–198.

53. Sutcliffe JG, Hedlund PB, Thomas EA, Bloom FE, Hilbush BS. Peripheral reduction of beta-amyloid is sufficient to reduce brain beta-amyloid: Implications for Alzheimer's disease. *J Neurosci Res.* 2011;89(6):808–814.

54. Mackic JB, et al. Circulating amyloid-beta peptide crosses the blood-brain barrier in aged monkeys and contributes to Alzheimer's disease lesions. *Vascul Pharmacol.* 2002;38(6):303–313.

55. Kalea AZ, Reiniger N, Yang H, Arriero M, Schmidt AM, Hudson BI. Alternative splicing of the murine receptor for advanced glycation end-products (RAGE) gene. *FASEB J.* 2009;23(6):1766–1774.

56. Arancio O, et al. RAGE potentiates Abeta-induced perturbation of neuronal function in transgenic mice. *EMBO J.* 2004;23(20):4096–4105.

57. El Khoury J, et al. Ccr2 deficiency impairs microglial accumulation and accelerates progression of Alzheimer-like disease. *Nat Med.* 2007;13(4):432–438.

58. Hickman SE, Allison EK, El Khoury J. Microglial dysfunction and defective beta-amyloid clearance pathways in aging Alzheimer's disease mice. *J Neurosci.* 2008;28(33):8354–8360.

59. Janelsins MC, et al. Chronic neuron-specific tumor necrosis factor-alpha expression enhances the local inflammatory environment ultimately leading to neuronal death in 3xTg-AD mice. *Am J Pathol.* 2008;173(6):1768–1782.

60. Shibata M, et al. Clearance of Alzheimer's amyloid-ss(1-40) peptide from brain by LDL receptor-related protein-1 at the blood-brain barrier. *J Clin Invest.* 2000;106(12):1489–1499.

61. Kayed R, et al. Common structure of soluble amyloid oligomers implies common mechanism of pathogenesis. *Science.* 2003;300(5618):486–489.

62. Ohno K, Pettigrew KD, Rapoport SI. Lower limits of cerebrovascular permeability to nonelectrolytes in the conscious rat. *Am J Physiol.* 1978; 235(3):H299–H307.

63. Sagare A, et al. Clearance of amyloid-beta by circulating lipoprotein receptors. *Nat Med.* 2007;13(9):1029–1031.

64. Mumby DG, Gaskin S, Glenn MJ, Schramek TE, Lehmann H. Hippocampal damage and exploratory preferences in rats: memory for objects, places, and contexts. *Learn Mem.* 2002;9(2):49–57.

65. Winters BD, Bussey TJ. Transient inactivation of perirhinal cortex disrupts encoding, retrieval, and consolidation of object recognition memory. *J Neurosci.* 2005;25(1):52–61.

66. Shichinohe H, et al. Neuroprotective effects of the free radical scavenger Edaravone (MCI-186) in mice permanent focal brain ischemia. *Brain Res.* 2004;1029(2):200–206.

67. Lanz TA, Hosley JD, Adams WJ, Merchant KM. Studies of Abeta pharmacodynamics in the brain, cerebrospinal fluid, and plasma in young (plaque-free) Tg2576 mice using the gamma-secretase inhibitor N2-[(2S)-2-(3,5-difluorophenyl)-2-hydroxyethanoyl]-N1-[(7S)-5-methyl-6-oxo -6,7-dihydro-5H-dibenzo[b,d]azepin-7-yl]-L-alaninamide (LY-411575). *J Pharmacol Exp Ther.* 2004;309(1):49–55.